Asymmetry of the neutrino mean free path in partially spin polarized neutron matter within the Skyrme model

E. Bauer [1,2] and J. Torres Patiño[1]
[1]*IFLP, CCT La Plata, CONICET, La Plata, Argentina*
[2]*Facultad de Ciencias Astronómicas y Geofísicas, Universidad Nacional de La Plata, La Plata, Argentina*

(Received 13 January 2020; revised manuscript received 7 April 2020; accepted 9 June 2020; published 29 June 2020)

The asymmetry in the neutrino mean free path for the absorption reaction $\nu + n \to e^- + p$ is evaluated within hot neutron matter under a strong magnetic field. We consider densities in the range $0.05 \leqslant \rho \leqslant 0.4\,\mathrm{fm}^{-3}$, several temperatures up to 30 MeV, and magnetic field strengths from $B = 0$ up to $B = 10^{18}$ G. Polarized neutron matter is described within the nonrelativistic Hartree-Fock model using the LNS Skyrme interaction. The neutrino mean free path has a weak dependence on the temperature and, in the strong magnetic field region, it decreases for growing values of it. This contrasts with the scattering reaction $\nu + n \to \nu' + n'$, where the average mean free path is almost independent of the magnetic field and has a strong dependence on the temperature. We have evaluated the asymmetry from both the absorption and scattering reactions. Our results shows that the total asymmetry depends on the magnetic field intensity, the density, and the temperature. For a density of $0.16\ \mathrm{fm}^{-3}$ and for a magnetic field strength of $B = 10^{17}$ G, the asymmetries in the mean free path are found to be ≈9% and ≈3.4% for temperatures of $T = 15$ and 30 MeV, respectively. The same set of asymmetries for $B = 10^{18}$ G is ≈58% and ≈48%.

DOI: 10.1103/PhysRevC.101.065806

I. INTRODUCTION

Neutrinos play an important role in the evolution of stellar objects. The physics of neutrinos is relevant at all stages of stellar evolution, starting from supernova explosions [1–3]. After such an event, the remaining matter forms a compact object where the neutrinos are one of the key elements for understanding this process [4,5]. There are many mechanisms which produce neutrinos in a neutron star. The possible reactions depend on the neutron star region under consideration. In the neutron star crust one has electron-positron annihilation, plasmon decay, and electron-nucleus bremsstrahlung, among other phenomena. In the neutron star core, we mention just a few of all the possible reactions: baryon direct Urca, baryon modified Urca, baryon bremsstrahlung, and Coulomb bremsstrahlung. All this mechanisms, together with complete review on this subject, are discussed in detail in [6] (and references therein).

Certainly, the emission of neutrinos is considered the main mechanism for neutron star cooling in its early stages [7,8]. In the analysis of this emission, the neutrino mean free path λ is of central importance. Depending on the conditions of density and temperature, the neutrino mean free path ranges from small values, compared with the neutron star radius, up to very large values. In the absence of magnetic field this has been extensively discussed in the literature (see for instance [9–22]). The neutrino mean free path tells us about the neutrino emissivity from the neutron star and therefore the degree of cooling of the compact object.

The addition of a strong magnetic field modifies these processes. Observational data on the magnetic field strength in the neutron star surface indicates that this magnitude varies within the range $B = 10^8 - 10^{15}$ G. A comprehensive and detailed review of the magnetic field in neutron stars can be found in [23] and references therein. The magnetic field strength in the surface of a neutron star such as a young radiopulsar ($\tau \approx 10^3\ 10^7$ yr) has values in the range $B = 10^{11} - 10^{13}$ G. For an old radiopulsar ($\tau \approx 10^8$–10^{10} yr) this value decrease to $B = 10^8 - 10^9$ G, while in the surface of a magnetar this value rises up to $B \approx 10^{15}$ G and it can grow by several orders of magnitude in its dense interior [24]. The stability condition requiring that the total neutron star energy be negative leads to an upper bound on the magnetic field strength of $B \lesssim 10^{18}$ G [25].

According to some authors, the magnetic field establishes an asymmetry in the emission of neutrinos [26–38]. This asymmetry has astrophysical implications, and perhaps the most important one is as a possible mechanism for the explanation of the "pulsar kick problem": the observation that a pulsar does not move with the velocity of its progenitor star, but rather with a substantially greater speed. Even though this model has been objected to as the only source to explain the problem of pulsar kick (see for instance [39]), an asymmetry of ≈1% would be enough to understand this behavior [27]. There are two main mechanisms responsible for this asymmetry. One is the effect of the magnetic field on the oscillation of the neutrinos [26]. The second source of asymmetry is the parity violation reactions which take place inside the neutron star [27–38]. This last approach is the one that we adopt in this work.

In this work we analyze the asymmetry in the neutrino mean free path for the absorption reaction $\nu + n \to e^- + p$, in

hot dense neutron matter. In a previous paper we discussed the scattering process $\nu + n \to \nu' + n'$ [38]. By considering both reactions, the asymmetry in the neutrino emission can originate from the differential cross section and from the neutrino mean free path (which is the inverse of the total cross section per unit volume). These two mechanism are independent and should be considered simultaneously to account for the actual asymmetric neutrino emission. While the first one is restricted to the scattering reaction and it gives us information on the way in which the weak interaction scatters the neutrinos, for the mean free path both reactions are present and it tells us about how often a neutrino interacts with a neutron. We consider that the mean free path is the relevant variable in this problem: if the mean free path is much larger than the size of the compact object itself, then the asymmetry in the differential cross section would not act, since it would be unlikely to have a collision.

As we have already mentioned, we analyze the absorption reaction which takes place in hot dense neutron matter under a strong magnetic field, which we consider as locally constant. In free space, the total neutrino cross section shows a dependence on the angle of the incoming neutrino with respect to the magnetic field [34]. In addition, for a dense medium the magnetic field induces some degree of polarization of the neutron matter, which also contributes to the asymmetry in the neutrino cross section (or equivalently to the neutrino mean free path). Neutron matter is described using the equation of state (EoS) developed in [40,41]. In this approach, the EoS is developed based on the Hartree—Fock approximation using the nuclear interaction given by the non–relativistic Skyrme potential model. In this sense we present a self-consistent treatment of the problem: we evaluate the neutron single-particle energy, its chemical potential, and the spin polarization of the neutron matter from the EoS, and these values are employed in the evaluation of the neutrino mean free path. This model for the EoS is particularly suitable for our problem. This is because we obtain an explicit expression for the neutron single-particle energy, which simplifies the evaluation of the neutrino mean free path. More details on this point are given in the following sections.

This work is organized as follows. In Sec. II we present the formalism for the neutrino mean free path. This is done in two subsections where we discuss the EoS in first place and then we give some details on the derivation of the cross section per unite volume. In the next step, we discuss our results in Sec. III, where we also include the scattering mean free path previously evaluated. Finally, in Sec. IV we give some conclusions.

II. THE NEUTRINO ABSORPTION CROSS SECTION

In this section we present an expression for the neutrino absorption cross section in hot neutron matter under a strong constant magnetic field. Much of the information in this section has been published in other works, and we have done a summary of them for the convenience of the reader. But also we add some specific information which should be given in the context of our problem.

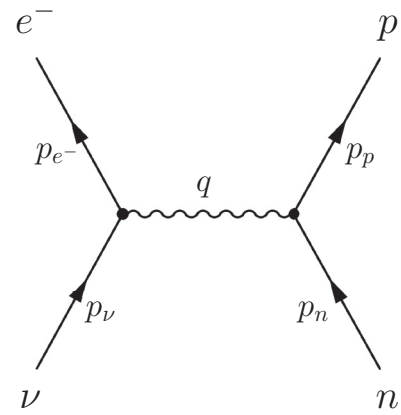

FIG. 1. The lowest order Feynman diagram for the absorption reaction $\nu + n \to e^- + p$. The quantities p_i and q denote, respectively, the four-momentum of the involved particles and the corresponding four-momentum transfer by the interaction.

The reaction under consideration is the absorption of a neutrino by a neutron, having an electron and a proton as the final state,

$$\nu + n \to e^- + p, \tag{1}$$

where the Feynman diagram for this reaction is drawn in Fig. 1. This reaction can take place either in free space or within a dense medium. We are considering pure hot non-relativistic neutron matter, and to evaluate the cross section we need two basic elements: first, a model for the neutron matter. This means that we have to develop an equation of state (EoS) for the dense medium under the influence of a strong magnetic field, from which we obtain the physical state of the system, characterized by the polarization, the single-particle energies, and the chemical potential for equilibrium. The second element is the evaluation of the diagram in Fig. 1 itself, using the standard rules for the evaluation of diagrams. For the interaction which mediates this reaction, we employ an effective Hamiltonian which is the low-momentum limit of the weak vertex from the standard model. In the following two subsections we address these points.

A. The EoS model using a Skyrme interaction

The EoS is evaluated using Hartree-Fock approximation with the Skyrme interaction [40,41]. We assume a system of neutrons within a strong magnetic field at finite temperature. The neutrons interact through the strong interaction among each other and with the external magnetic field. From the EoS, we obtain the degree of polarization of the system, the single-particle energies of the neutrons, and their chemical potential. This is done by giving the density of the system, its temperature, and the intensity of the magnetic field, which we consider as a constant field in the $\hat{z}$ direction. This hypothesis on the magnetic field is not an important restriction as it should be employed locally (as should the density and the temperature). For the whole neutron star one can implement a realistic model for the magnetic field. The curvature of such a

field would allow us to consider it as locally uniform due to the scale of the neutrino-neutron absorption reaction.

Now we briefly describe how we obtain the different outcomes from the EoS. For a more detailed analysis we refer the reader to [38,40,41]. The starting point is to define the adequate thermodynamical potential for our problem. For a system within a magnetic field $\vec{B}$, we employ

$$\mathcal{U} = \mathcal{F} - \vec{\mathcal{M}} \cdot \vec{B}, \tag{2}$$

where $\mathcal{F}$ and $\vec{\mathcal{M}}$ are, respectively, the Helmhotz free energy density and the magnetization per unit volume of the system. The expression for the density of the system is given by

$$\rho = \sum_{s_n=\pm 1} \frac{1}{(2\pi)^3} \int d^3p_n f_{s_n}(E_n, \mu_n, T). \tag{3}$$

Here E_n, μ_n, and T stand for the neutron single-particle energy, its chemical potential, and the temperature, respectively. The function $f_{s_n}(E_n, \mu_n, T)$ in thermal equilibrium is given by the Fermi-Dirac particle distribution function,

$$f_{s_i}(E_i, \mu_i, T) = \frac{1}{1 + \exp[\{E_i - \mu_i(T)\}/T]}. \tag{4}$$

It is straightforward to define the spin up and down partial densities as ρ_+ and ρ_-, respectively, where for the total density we have $\rho = \rho_+ + \rho_-$. The spin asymmetry is

$$A = \frac{1}{\rho} \sum_{s_n=\pm 1} \frac{s_n}{(2\pi)^3} \int d^3p_n f_{s_n}(E_n, \mu_n, T), \tag{5}$$

or, equivalently, $A = (\rho_+ - \rho_+)/(\rho_+ + \rho_+)$. At this point it is convenient to give the expression for the neutron single-particle energy, E_n. Using the Hartree-Fock model with the Skyrme interaction, we have [40,41]

$$E_n = m_n + \frac{p_n^2}{2m^*_{s_n}} - s_n \mu_{Bn} B + \frac{v_{s_n}}{8}, \tag{6}$$

where $\mu_{Bn} = -1.913\mu_N$ is the anomalous magnetic moment of the neutron in units of the nuclear magneton μ_N. The potential term, v_{s_n} depends on the density, the temperature, and the magnetic field, but not on the momentum, and it is given by

$$v_{s_n} = a_0(1 - s_n A)\rho + 2(b_0 + s_n b_1)\,\mathcal{K}_{s_n=1}, \tag{7}$$

where

$$\mathcal{K}_{s_n} = \frac{1}{(2\pi)^3} \int d^3p\, p^2 f_{s_n}(E_n, \mu_n, T). \tag{8}$$

The constants $a_0 = 4t_0(1 - x_0) + 2t_3\rho^\sigma(1 - x_3)/3$, $b_0 = t_1(1 - x_1) + 3t_2(1 + x_2)$, and $b_1 = -t_1(1 - x_1) + t_2(1 + x_2/2)$ are written in terms of the standard parameters of the Skyrme model, $t_0, t_1, t_2, x_0, x_1, x_2$, and σ. In Eq. (6), for the effective mass we have

$$\frac{1}{m^*_s} = \frac{1}{m_n} + \frac{1}{4}\rho\,(b_0 + s\,b_1\,A). \tag{9}$$

The chemical potential corresponding to the physical state does not depend on the spin projection of the neutron due to the minimization process. To see this point we write

$$\mu_{s_n} = \frac{\partial \mathcal{U}}{\partial \rho_{s_n}}. \tag{10}$$

This expression can be rewritten in terms of the spin asymmetry A as

$$\mu_{s_n} = \frac{\partial \mathcal{U}}{\partial \rho} + s_n \left(\frac{1 - s_n A}{\rho}\right) \frac{\partial \mathcal{U}}{\partial A}. \tag{11}$$

The difference between the two chemical potentials is then

$$\mu_+ - \mu_- = \frac{2}{\rho} \frac{\partial \mathcal{U}}{\partial A}, \tag{12}$$

which shows that the minimization of $\mathcal{U}$ with respect to A implies the existence of a unique chemical potential in the physical state. We should emphasized that this minimization is performed with the constrain of a fixed density. This is a self-consistent process: we need μ_n to evaluate ρ_+ and ρ_-, which defines the spin asymmetry A, needed in the single-particle energy, etc. Summarizing, given the density, temperature, and the magnetic field of the system, from the EoS we obtain the actual physical state, characterized by the chemical potential, the single-particle energies of the neutrons, and the spin asymmetry which is a global property of the system.

B. The absorption neutrino cross section for a polarized system

In this subsection we show an expression for the absorption neutrino cross section per unit volume for a polarized system. The formalism of this subsection is taken from the work by Arras and Lai [42]. We summarized the formalism for convenience and we also add some particular expressions not given in [42], that we need in our work.

The aim of this subsection is to write the expression for the mean free path for the absorption reaction $\nu + n \to e^- + p$, depicted in Fig. 1. The total absorption cross section per unit volume can be written as

$$\frac{\sigma_{\rm abs}}{V} = \int d\Pi_p\, d\Pi_e\, d\Pi_n\, \mathcal{W}^{\rm abs}_{\rm fi} \left[1 - f_{s_p}(E_p, \mu_p, T)\right] \times \left[1 - f_{s_e}(E_e, \mu_e, T)\right] f_{s_n}(E_n, \mu_n, T). \tag{13}$$

The expressions for $\int d\Pi_j$ are given in Appendix A. The function $\mathcal{W}^{\rm abs}_{\rm fi}$ is the transition rate, where the indexes i and f are the initial and final states respectively. Our initial state has a neutrino and a neutron, and the final state has an electron and a proton. To evaluate the transition rate we first give the expression for the scattering operator $\hat{S}$. This operator is expressed in terms of the time-evolution operator $\hat{U}(t_2, t_1)$, as $\hat{S} = \hat{U}(-\infty, \infty)$ [43]. Following this reference and by keeping only the leading term, we have

$$\hat{S} = i \int d^4x\, \hat{\mathcal{H}}_{\rm int}, \tag{14}$$

where $\hat{\mathcal{H}}_{\rm int}$ is the Hamiltonian density. We employ an effective Hamiltonian which is the low-momentum limit of the weak vertex from the standard model (see for instance [16]),

$$\hat{\mathcal{H}}_{\rm int} = \frac{G_F}{\sqrt{2}} \bar{\Psi}_p \gamma_\mu (g_V - g_A\gamma_5) \Psi_n\, \bar{\Psi}_e \gamma^\mu (1 - \gamma_5) \Psi_\nu + \text{H.c.} \tag{15}$$

Here G_F is the Fermi weak coupling constant $[G_F/(\hbar c)^3 = 1.16637(1) \times 10^{-5}\ \text{GeV}^{-2}]$. For the vector and axial-vector couplings we have $g_V = 0.973$ and $g_A = 1.197$, respectively.

The scattering matrix S_{fi}, is $\hat{S}$-operator evaluated between the initial and final states. The square of S_{fi}, divided by time is the transition rate:

$$\mathcal{W}_{\text{fi}}^{\text{abs}} = \frac{|\, S_{\text{fi}}\,|^2}{\mathcal{T}}, \tag{16}$$

where $\mathcal{T}$ is the time interval where the transition takes place [44].

The wave functions for all particles are given in the Appendix A. Wave functions are expressed in cylindrical coordinates (ρ, ϕ, z) and in this Appendix we also define some functions and constants employed in the present section. Using these wave functions together with the interaction in Eq. (15), the S_{fi} matrix is given by

$$\begin{aligned} S_{\text{fi}} = -i\frac{G_F}{\sqrt{2}} L^{-1}V^{-1}(2\pi)^2\delta(E_e + E_p - |p_\nu| - E_n) \\ \times \delta(p_{e,z} + p_{p,z} - p_{\nu,z} - p_{n,z}) \\ \times \left(\frac{eB}{2\pi}\right)\int_0^\infty d\rho\,\rho \int_0^{2\pi} d\phi\, e^{i\vec{\omega}_\perp\cdot\vec{x}_\perp} \\ \times e^{i(N_e-R_e)\phi}\, e^{-i(N_p-R_p)\phi}\bar{U}_p\gamma_\mu(g_V - g_A\gamma_5)U_n \\ \times \bar{U}_e\gamma^\mu(1-\gamma_5)U_\nu, \end{aligned} \tag{17}$$

where $\vec{\omega}_\perp = (p_{n,x} + p_{\nu,x})\,\hat{i} + (p_{n,y} + p_{\nu,y})\,\hat{j}$ and $\vec{x}_\perp = x\,\hat{i} + y\,\hat{j}$. Here $V = L\mathcal{A}$ is the wave function normalization volume, where L is the length along the z axis and $\mathcal{A}$ is the area in the perpendicular plane. The spinors U_j are defined in Appendix A, together with more details on the normalization volume. To square the modulus of this expression we employ the property

$$\begin{aligned} &\delta^2(E_e + E_p - |p_\nu| - E_n) \\ &\quad = \delta(E_e + E_p - |p_\nu| - E_n)\,\frac{\mathcal{T}}{2\pi}, \\ &\delta^2(p_{e,z} + p_{p,z} - p_{\nu,z} - p_{n,z}) \\ &\quad = \delta(p_{e,z} + p_{p,z} - p_{\nu,z} - p_{n,z})\,\frac{L}{2\pi}. \end{aligned} \tag{18}$$

The transition rate is written as

$$\begin{aligned} \mathcal{W}_{\text{fi}}^{\text{abs}} = L^{-1}V^{-2}(2\pi)^2\delta(E_e + E_p - |p_\nu| - E_n) \\ \times \delta(p_{e,z} + p_{p,z} - p_{\nu,z} - p_{n,z})\ |\, M\,|^2, \end{aligned} \tag{19}$$

where we have defined

$$\begin{aligned} |\, M\,|^2 = \frac{G_F^2}{2}\left(\frac{eB}{2\pi}\right)^2 \Bigg| \int_0^\infty d\rho\,\rho \\ \times \int_0^{2\pi} d\phi\, e^{i\vec{\omega}_\perp\cdot\vec{x}_\perp}\, e^{i(N_e-R_e)\phi}\, e^{-i(N_p-R_p)\phi} \\ \times \bar{U}_p\gamma_\mu(g_V - g_A\gamma_5)U_n\bar{U}_e\gamma^\mu(1-\gamma_5)U_\nu\Bigg|^2. \end{aligned} \tag{20}$$

The integration over the cylindrical coordinates ρ and ϕ can be done using the relations (4.6) and (4.7) in [45], Chap. 2:

$$\int_0^{2\pi}\frac{d\phi}{2\pi}\, e^{i\vec{\omega}_\perp\cdot\vec{x}_\perp}\, e^{i(N_e-R_e)\phi}\, e^{-i(R_p-N_p)\phi} = J_{N_e-R_e-(N_p-R_p)}(\omega_\perp\rho), \tag{21}$$

where $J_n(x)$ is the nth Bessel function and

$$\begin{aligned} \int_0^\infty d\rho\,\rho\, I_{N_e,R_e}(\xi)I_{Rp,Np}(\xi)J_{N_e-R_e-(N_p-R_p)}(\omega_\perp\rho) \\ = \frac{(-1)^{N_p-R_p}}{eB} I_{N_e,N_p}\left(\frac{\omega_\perp^2}{2eB}\right) I_{R_e,R_p}\left(\frac{\omega_\perp^2}{2eB}\right). \end{aligned} \tag{22}$$

Using these integrals, Eq. (20) is given by

$$\begin{aligned} |\, M\,|^2 = \frac{G_F^2}{2}\, I_{R_e,R_p}^2\left(\frac{\omega_\perp^2}{2eB}\right) \\ \times |\overline{\widetilde{U}}_p\gamma_\mu(g_V - g_A\gamma_5)U_n\overline{\widetilde{U}}_e\gamma^\mu(1-\gamma_5)U_\nu|^2, \end{aligned} \tag{23}$$

where

$$\widetilde{U}_p = \begin{pmatrix} \delta_{s_p,+1} \\ \delta_{s_p,-1} \\ 0 \\ 0 \end{pmatrix} \quad \text{and} \quad \widetilde{U}_e = \begin{pmatrix} C_1 I_{N_e-1,N_p}(\omega_\perp^2/2eB) \\ iC_2 I_{N_e,N_p}(\omega_\perp^2/2eB) \\ C_3 I_{N_e-1,N_p}(\omega_\perp^2/2eB) \\ iC_4 I_{N_e,N_p}(\omega_\perp^2/2eB) \end{pmatrix}. \tag{24}$$

Note that in Eq. (23) all the R_e and R_p dependence is in the function I_{R_e,R_p}^2. From Eq. (11.7) in [45], we have

$$\sum_{R_e=0}^{R_{e,\max}}\sum_{R_p=0}^{R_{p,\max}} I_{R_e,R_p}^2 = \sum_{R_e=0}^{R_{\max}} 1 = R_{\max} = \mathcal{A}\,\frac{eB}{2\pi}, \tag{25}$$

where $R_{e,\max} = R_{p,\max} = R_{\max}$ is discussed in Appendix A. From this, we can write

$$\sum_{R_e=0}^{R_{\max}}\sum_{R_p=0}^{R_{\max}}\sum_{\sigma_e=\pm1} c(N_e,\sigma_e)\ |\, M\,|^2 = \frac{G_F^2}{2}\,\mathcal{A}\,\frac{eB}{2\pi}\,L_{\mu\nu}N^{\mu\nu}, \tag{26}$$

where $L_{\mu\nu}$ and $N^{\mu\nu}$ are the lepton and hadron tensors, respectively. Their expressions are

$$\begin{aligned} L_{\mu\nu} &= \sum_{\sigma_e=\pm1} c(N_e,\sigma_e)\,\overline{\widetilde{U}}_e\,\gamma_\mu(1-\gamma_5)\,U_\nu\,\overline{U}_\nu\gamma_\nu(1-\gamma_5)\widetilde{U}_e, \\ N^{\mu\nu} &= \overline{\widetilde{U}}_p\gamma^\mu(g_V - g_A\gamma_5)U_n\overline{U}_n\gamma^\nu(g_V - g_A\gamma_5)\widetilde{U}_p. \end{aligned} \tag{27}$$

The next step is to build the transition rate $\mathcal{W}_{\text{fi}}^{\text{abs}}$, and insert it into Eq. (13). We also have to replace $\int d\Pi_e$, $\int d\Pi_p$ and $\int d\Pi_n$ by Eqs. (A8), (A12), and (A17), respectively. The final expression is given by

$$\begin{aligned} \frac{\sigma_{\text{abs}}}{V} = \frac{G_F^2}{2}\,\frac{eB}{2\pi}\sum_{N_e=0}^{N_{e,\max}}\int_{-\infty}^{\infty}\frac{d\,p_{e,z}}{2\pi}[1 - f_{s_e}(E_e,\mu_e,T)] \\ \times \sum_{N_p=0}^{N_{p,\max}}\int_{-\infty}^{\infty}\frac{d^2p_{n,\perp}}{(2\pi)^2}\sum_{s_p=\pm1} \\ \times\Bigg[\left(\frac{1+A}{2}\right)S_{s_p,s_n,N_p,N_e}L_{\mu\nu}N^{\mu\nu}\ |_{s_n=1} \\ + \left(\frac{1-A}{2}\right)S_{s_p,s_n,N_p,N_e}L_{\mu\nu}N^{\mu\nu}\ |_{s_n=-1}\Bigg], \end{aligned} \tag{28}$$

where $p_{n,\perp} = \sqrt{p_{n,x}^2 + p_{n,y}^2}$. The existence of maximum values for N_p and N_e is analyzed in Appendix B. Note that,

due to the importance that we assign to the equation of state, we have already split this expression into terms with the neutron spin up and down, respectively. Each term is weighed by the corresponding spin asymmetry factor. This is a result from our definition for the neutron spinor in Eq. (A16). Thanks to the presence two Kronecker deltas in this spinor, no modification is required in the hadron tensor. In Eq. (28), we have introduced the structure function for the absorption process as

$$\begin{aligned} S_{s_p,s_n,N_p,N_e} = & \int_{-\infty}^{\infty} \frac{dp_{n,z}}{2\pi} \int_{-\infty}^{\infty} \frac{dp_{p,z}}{2\pi} (2\pi)^2 \\ & \times \delta(E_e + E_p - |p_\nu| - E_n) \\ & \times \delta(p_{e,z} + p_{p,z} - p_{\nu,z} - p_{n,z}) \\ & \times f_{s_n}(E_n, \mu_n, T)\left[1 - f_{s_p}(E_p, \mu_p, T)\right]. \end{aligned} \tag{29}$$

An analytical expression for this function is given in Appendix C, where unlike in [42] this function is evaluated in the case where $m_p \neq m_n$. This is because the use of an effective mass does not allow the approximation $m_p \cong m_n$. It is important to notice that the integration of Eq. (29), shown in Appendix C, is valid only for the Skyrme model and also for a Fermi sea of noninteracting particles: a system where single-particle energies can be written in the form of Eqs. (C2). From the models for the EoS where single-particle energies are obtained numerically, a numerical integration of Eq. (29) [in fact, of Eq. (C4)] should be done, which makes the numerical problem much more difficult due to the usually big values for the N_p summation in Eq. (28).

Finally, the contraction of the leptonic and hadronic currents are given by

$$\begin{aligned} L_{\mu\nu}N^{\mu\nu}\,|_{s_p,s_n}\,(N_e = 0) = \theta(p_{e,z})\, I^2_{0,N_p}(t)\, \big\{ & g_V^2 + 3g_A^2 + \left(g_V^2 - g_A^2\right)\cos(\theta_\nu) + 2g_A(g_A + g_V)[s_p + s_n\cos(\theta_\nu)] \\ & - 2g_A(g_A - g_V)[s_n + s_p\cos(\theta_\nu)] + \left[g_V^2 - g_A^2 + \left(g_V^2 + 3g_A^2\right)\cos(\theta_\nu)\right] s_n s_p \big\}, \end{aligned} \tag{30}$$

where θ_ν is the angle between the neutrino and the magnetic field. When $N_e \geqslant 1$, we have

$$\begin{aligned} L_{\mu\nu}N^{\mu\nu}\,|_{s_p,s_n}\,(N_e \geqslant 1) = {} & g_V^2 \left\{ I^2_{N_e-1,N_p}(t)\Sigma^-_{N_e}(p_{e,z})[1 - \cos(\theta_\nu)] + I^2_{N_e,N_p}(t)\Sigma^+_{N_e}(p_{e,z})[1 + \cos(\theta_\nu)] \right\}(1 + s_n s_p) \\ & + g_A^2 \left\{ I^2_{N_e-1,N_p}(t)\Sigma^-_{N_e}(p_{e,z})\,[3 + \cos(\theta_\nu) + 2(s_n - s_p)(1 + \cos(\theta_\nu)) - s_n s_p(1 + 3\cos(\theta_\nu))] \right. \\ & \left. + I^2_{N_e,N_p}(t)\Sigma^+_{N_e}(p_{e,z})\,[3 - \cos(\theta_\nu) - 2(s_n - s_p)(1 - \cos(\theta_\nu)) - s_n s_p(1 - 3\cos(\theta_\nu))] \right\} \\ & + 2g_V g_A \left\{ I^2_{N_e-1,N_p}(t)\Sigma^-_{N_e}(p_{e,z})[-1 + \cos(\theta_\nu)] + I^2_{N_e,N_p}(t)\Sigma^+_{N_e}(p_{e,z})[1 + \cos(\theta_\nu)] \right\}(s_n + s_p), \end{aligned} \tag{31}$$

where

$$\Sigma^\pm_{N_e}(p_{e,z}) \equiv \frac{1}{2}\left(1 \pm \frac{p_{e,z}}{\left|\left(p_{e,z}^2 + 2eBN_e\right)^{1/2}\right|}\right). \tag{32}$$

The expression in Eq. (30) is the same as the one in [42]. But for the one in Eq. (31) we have considered all spin terms. Note that the neutrino mean free path is obtained from the cross section as $\lambda_{\rm abs} = (\sigma_{\rm abs}/V)^{-1}$. In the next section we discuss our results.

Note that, because in this work we employ pure neutron matter, once the neutrino is absorbed by the neutron, the final proton and electron do not find other fermions of the same kind. In this sense, in Eq. (13) [or Eqs. (28) and (29)], we should make the replacements $[1 - f_{s_p}(E_p, \mu_p, T)] \to 1$ and $1 - f_{s_e}[E_e, \mu_e, T)] \to 1$. However, we have retained these functions to preserve a more general scheme.

III. RESULTS AND DISCUSSION

We present now our results for the neutrino mean free path in homogeneous hot neutron matter under the presence of a strong magnetic field. We consider a range of densities of $0.04 \leqslant \rho \leqslant 0.4$ fm^{-3}, corresponding approximately to the outer core region of a neutron star, temperatures up to $T = 30$ MeV, and different values of the magnetic field intensity ranging from $B = 0$ up to $B = 10^{18}$ G. The EoS is evaluated within the Hartree-Fock model, using LNS Skyrme interaction developed by Cao *et al.* [46]. We have developed our formalism assuming a particular form for the single-particle energy for the neutron, which is the one from the Skyrme model. This expression is shown in Eq. (6). In [38] we have employed the same model together with the Brueckner-Hartree-Fock (BHF) approach using the Argonne V18 [47] nucleon-nucleon potential supplemented with the Urbana IX [48] three-nucleon force. In that work we have obtained a good agreement between both models for the inelastic dispersion of neutrinos by neutrons. Note that the LNS Skyrme interaction is specially suitable for a comparison with the BHF model, since its parameters were determined by fitting the nuclear matter EoS calculated in the BHF framework.

Before the discussion of our results, it is convenient to make a summary of the spin asymmetry of the system, which was already analyzed in [38] for the same interaction (see in particular Fig. 3 in that work). The spin asymmetry A characterizes the degree of polarization of the system. That is, we consider a system of neutrons interacting with each other through the strong interaction and with an external strong magnetic field. The strong interaction favors an equal number of neutrons with spin up and down (i.e., $A = 0$), while the magnetic field tries to align all the neutron spins antiparallel to it (i.e., $A = -1$). The actual value for A is then obtained through an energy minimization calculation from the EoS, as discussed in Sec. II A. As expected, the magnitude of A increases for decreasing densities and also for growing values of the magnetic field. In fact, within the range of B from 10^{14} G up to 2.5×10^{18} G, we have $\log_{10}(|\,A\,|) \cong a\log_{10}(B) + b$,

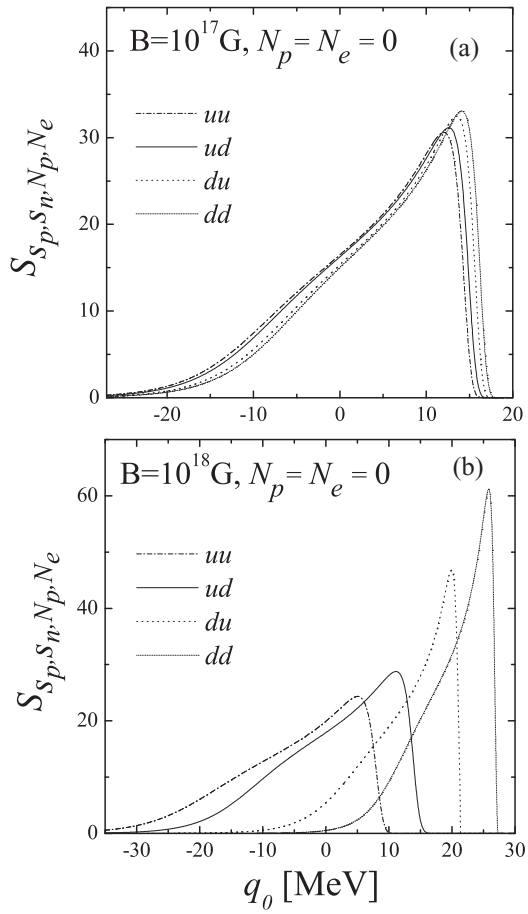

FIG. 2. Energy dependence of the structure function $\mathcal{S}_{s_p,s_n,N_p,N_e}$ for $\rho = 0.16$ fm^{-3}. In all panels we consider $N_p = N_e = 0$, we take $q_z > 0$ and $q_z \cong q_0 - |\vec{p}_\nu|[1 - \cos(\theta_\nu)]$, and we employ as a representative value for the square of the transverse momentum transfer by the neutron, $p_{n,\perp} = 170$ MeV. Also we use $|\vec{p}_\nu| = 3T$, with $T = 15$ MeV. The values for s_p, s_n are uu, ud, du, and dd. In panels (a) and (b) we show results for two values of the the magnetic field intensity, where we have used $\theta_\nu = 0$.

where $a \cong 1$ and b is approximately constant for a fixed value of the density (this behavior is depicted in panels (b) and (d) in Fig. 3 of [38]). Our concern in this work is the neutrino mean free path, which has different values according to the state of polarization of the neutron matter. This is developed in the following.

We turn now to the analysis of the absorption structure function as defined in Eq. (29). The expression for this structure function is given in Appendix C. At variance with the well studied structure function for the dispersion mean free path (see Eq. (23) in [38]), this structure function has some particular features which deserve to be discussed. One should keep in mind that our structure function represents only a fraction of the proton-neutron phase space and, due to this, it depends on many variables. Beyond its rather simple expression, it is the great number of independent variables which makes it difficult to analyze. Following the same pattern as for the dispersion structure function, we plot the absorption structure function as a function of q_0 (the energy transfer by the weak interaction). But instead of using a fixed value for q_z, we employ $q_z \cong q_0 - |\vec{p}_\nu|[1 - \cos(\theta_\nu)]$. This expression is obtained by solving the first two expressions in Eqs. (C6), for $q_z > 0$ and $E_e \cong p_{e,z}$.

In Fig. 2 we plot the structure function at a fixed density for different proton-neutron spin projections, denoted as $s_p, s_n = uu$, ud, du, and dd. In this figure we study the effect of the magnetic field on the structure function. The first obvious result is that the split among the different spin components is more relevant for $B = 10^{18}$ G. This split is due to two main elements. First, it is due to the coupling of the magnetic field with the magnetic moments of protons and neutrons: from Eqs. (C2) we notice that there is an energy shift of $\Delta E = (s_p\mu_{Bp} - s_n\mu_{Bn})B$. Keeping in mind that $\mu_{Bp} > 0$ and $\mu_{Bn} < 0$, the main source of this split is understood. Second, the neutron effective mass depends on its spin projection, which represents the second contribution to the split. However, due to the particular Skyrme model that we have employed, this effect is small. This is because the split between the spin up and down effective masses is small. Some parametrizations of the Skyrme interaction lead to a more important split among these two components (see for instance Fig. 5 in [41]). Note that in Fig. 5 in [41] the split is significant for $B = 10^{19}$ G, and it shows a considerable reduction for $B = 2.5 \times 10^{18}$ G. Due to the temperatures and the magnetic field strengths under consideration in this work, the coupling of the magnetic field with the magnetic moment of protons and neutrons is the dominant element to understand the results in Fig. 2.

The shape of the different structure functions is linked to the single-particle energies and to the chemical potential derived from the EoS. But it is the area under the different functions which really matters: comparing the different areas, the bigger ones leads to bigger cross sections and smaller mean free paths. Let us denote the different areas under each

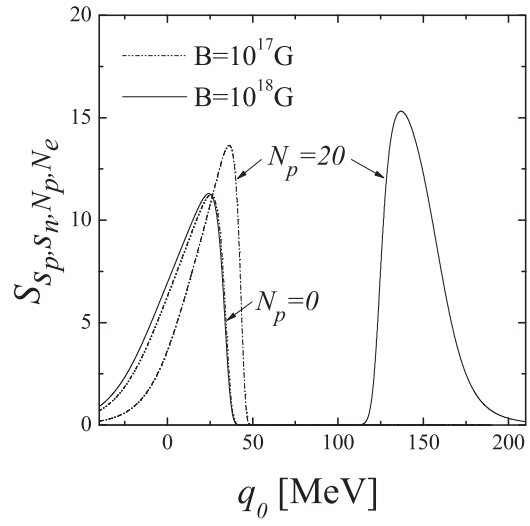

FIG. 3. Dependence of the structure function $\mathcal{S}_{s_p,s_n,N_p,N_e}$ on N_p for two values of the magnetic field intensity and $N_e = 0$. We have considered $\theta_\nu = \pi/2$, $p_{n,\perp} = 120$ MeV, $|\vec{p}_\nu| = 3T$, with $T = 30$ MeV and $s_p, s_n = ud$, while the other conditions are the same as in Fig. 2.

structure function as $\int S_{s_p,s_n,N_p,N_e}$. From Fig. 2 and assuming that the whole area contributes to the cross section, we notice that $\int S_{uu,0,0} < \int S_{ud,0,0}$ and $\int S_{du,0,0} < \int S_{dd,0,0}$: for a fixed proton spin projection, the contribution for neutrons with spin up is smaller than the one with spin down. The same behavior takes place for the dispersion structure function, having the same origin, which is the character of the phase space for polarization matter: the phase space for neutrons with spin up is smaller than that of neutrons with spin down. A complete discussion on this point is given in [38]. A corollary of this discussion is that the structure function has a clear spin dependence and, in the spin summation in Eq. (28), it cannot be taken as a common factor.

In the following two figures, we limit ourselves to one spin configuration for simplicity, as the other contributions have the same behavior. In Fig. 3, we show the N_p dependence of the structure function for two values of the magnetic field. By drawing the structure function for $N_p = 0$ and for $N_p = 20$, we observe an energy shift stemming from the $(N_p + 1/2)\, eB/m_p$ term in the proton single-particle energy. Because this term proportional to B, it is straightforward to understand that this shift is one order of magnitude bigger for $B = 10^{18}$ G than for $B = 10^{17}$ G. The problem here is, to what N_p value should we sum up? Or equivalently, what is the biggest value for q_0? The value for q_0 is limited by the conservation of energy: $|p_\nu| + E_n = E_e + E_p$. The initial energy of the system depends on the particular values of the momentum carried by each particle, its potential energy, and the value for the magnetic field. Note that $q_0 = |p_\nu| - E_e$: $|p_\nu|$ has a fixed value and $E_e < |p_\nu| + E_n$. This gives a maximum value for q_0, keeping in mind that $E_p \cong 0$ is not a realistic situation (see the discussion on the maximum value for the initial energy in Appendix B). This is the first constraint on the value for N_p, but as we discuss soon N_p has also restrictions due to the accessible phase space. Before ending this paragraph, it is worth mentioning that N_e is indirectly present in q_0. This quantum number is part of the electron single particle energy. In this figure, we have employed the approximate equality $q_z \cong q_0 - |\vec{p}_\nu|[1 - \cos(\theta_\nu)]$, which is valid only if $N_e = 0$. A similar figure can be done for $N_e \neq 0$, leading to the same conclusions.

In Fig. 4, which is the last one for the structure function, we consider the temperature dependence of this function for $B = 10^{18}$ G and for three values of the temperature, $T =$ 5, 15, and 30 MeV. By comparing these results with the ones from the dispersion structure function (see Fig. 4(a) in [38]), we notice that the behavior of the absorption structure function with temperature is quite different from the one in the dispersion process. For the dispersion process, the area under the structure function strongly grows with temperature. In contrast, for the absorption one the areas are similar, but with a clear decrease as one increases the temperature. The absorption structure function represents only a part of the available phase space and so gives a different result. A complete analysis of the temperature dependence requires the full phase space of the problem. This will be done soon, when we discuss the temperature dependence of the neutrino mean free path.

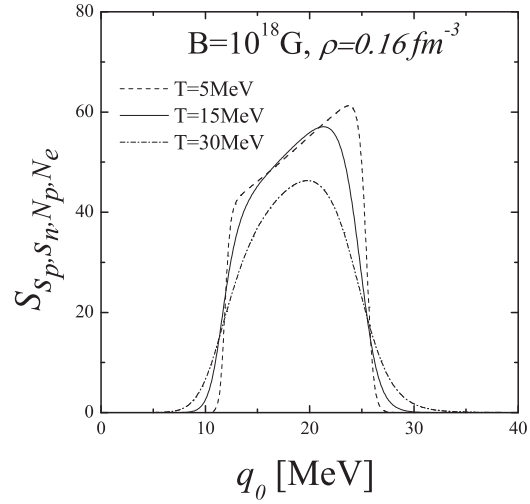

FIG. 4. The structure function $\mathcal{S}_{s_p,s_n,N_p,N_e}$ for different temperatures. We have considered $\theta_\nu = 0$, $p_{n,\perp} = 70$ MeV, $|\vec{p}_\nu| = 3T$, with $T = 30$ MeV and $s_p, s_n = ud$, while the other conditions are the same as in Fig. 2.

We have considered the absorption structure function in some detail, because it helps us to understand the mean free path. Another ingredient is the function $I^2_{N_e,N_p}(t)$ [see Eq. (A5)], which we have plotted in Fig. 5 for different values of N_p and N_e. As discussed in Sec. II, this function is part of the wave function of charged particles in a constant magnetic field: the energy levels are quantized for an axis perpendicular to the magnetic field direction and have continuum values parallel to the field. This is a function of $t = \omega^2_\perp/2eB$ and, in panel (a) of this figure, we consider different values for N_p with a fixed $N_e = 0$. In panel (b) we take $N_p = 100$ for two values of N_e. Our concern is how this function affects the result for the neutrino mean free path. Keeping in mind that $\int_0^\infty dt\, I^2_{N_e,N_p}(t) = 1$, the weight of this function is linked to the maximum value for t. The maximum value for $\omega_\perp = [(p_{n,x} + p_{\nu,x})^2 + (p_{n,y} + p_{\nu,y})^2]^{1/2}$ results from the particle distribution function $f_{s_n}(E_n, \mu_n, T)$ and the neutrino momentum. For the same $\omega^{\max}_\perp$, different values for the magnetic field give different $t^{\max}$. Together with the structure function, this $t^{\max}$ value establishes a constraint on the maximum values for N_p and N_e.

We turn now to the analysis of the neutrino absorption mean free path. We conclude our study by adding the dispersion contributions, which have been discussed in [38]. The behaviors of these two contributions with temperature and with magnetic field are very different. Due to this and for the benefit of the reader, we recall some aspects of the dispersion cross section in the following paragraphs. The presence of a constant magnetic field establishes a preferred direction in space and, consequently, the total cross section depends both on the magnitude of the momentum of the incoming neutrino and on the angle θ_ν between its momentum and the direction of the magnetic field. For the dispersion reaction, an incoming angle of $\theta_\nu = \pi/2$ results in a cross section almost identical to the one in the absence of the magnetic field. This is because the phase space for this reaction is barely modified by the

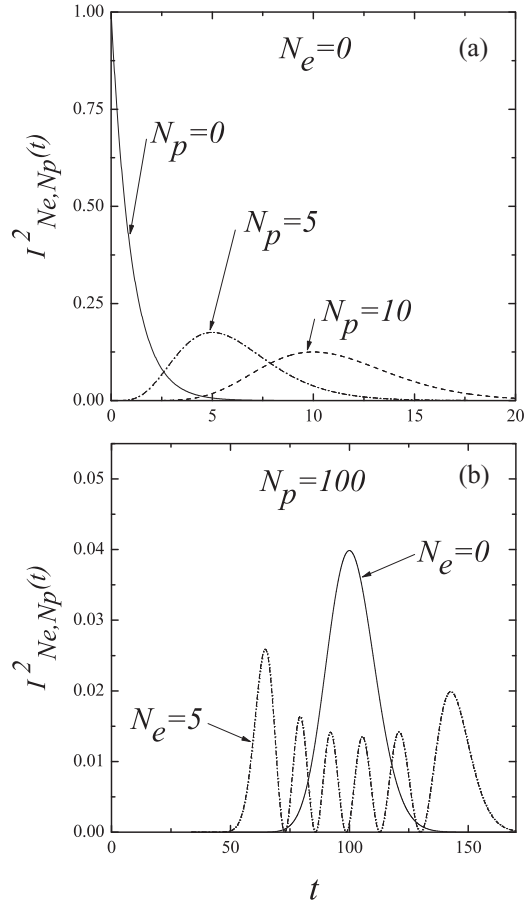

FIG. 5. Some values for the $I^2_{N_e,N_p}(t)$ function as defined in Eq. (A5).

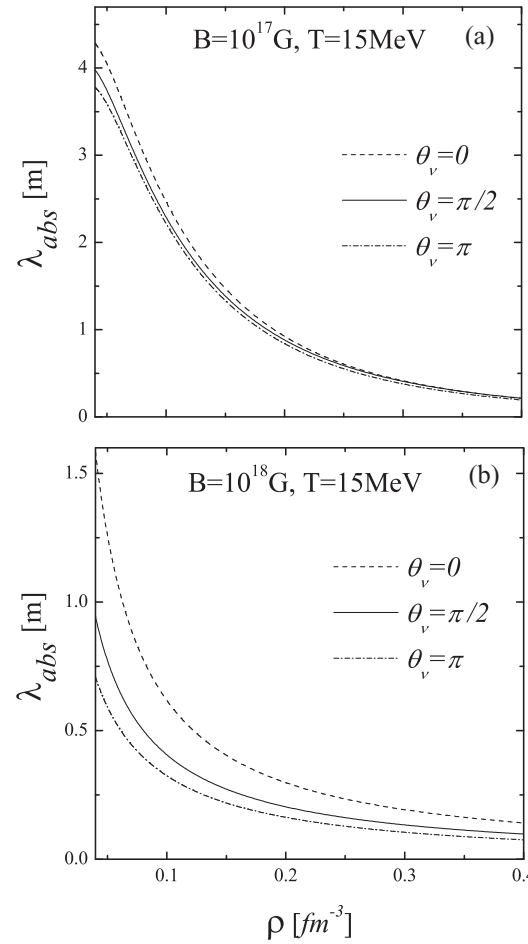

FIG. 6. The absorbtion neutrino mean free path as a function of the density and for three different values for the neutrino incoming angle, θ_ν. In panel (a) we show results for a magnetic field intensity $B = 10^{17}$ G, while we have $B = 10^{18}$ G for panel (b). The momentum of the incoming neutrino is $|\vec{p}_\nu| = 3T$.

magnetic field. As we show soon, this is not the case for the absorption reaction, where the phase space (of final states) is substantially modified by the magnetic field.

First, in Eq. (28) we sum over all spin components. By taking for simplicity the $N_e = 0$ case, the weak dynamics from Eq. (30) already gives us some relevant information about this sum. In Table I, we show results from Eq. (30), where we have used $g_V = 0.973$ and $g_A = 1.197$. From this table, we can see that contributions with spin down for the proton are zero for du and are almost negligible for dd. Moreover, for each of the two extreme values of θ_ν, only one spin component contributes to the cross section: the uu component for $\theta_\nu = 0$ and the ud component for $\theta_\nu = \pi$. Each component

TABLE I. Some values for the function $[L_{\mu\nu}N^{\mu\nu}/I^2_{0,N_p}(t)]$ $(s_p, s_n, \cos(\theta_\nu))$ from Eq. (30) for $p_{e,z} > 0$. Note that this function has no dimensions.

s_p, s_n	$\theta_\nu = 0$	$\theta_\nu = \pi/2$	$\theta_\nu = \pi$
uu	18.84	9.42	0
ud	0	11.46	22.92
du	0	0	$\approx$0
dd	0.20	0.10	0

is weighed by a different factor, even thought these factors are similar in magnitude. This fact, together with the different shapes for the spin components of the absorption structure function shown in Fig. 2, contribute to the asymmetry in the neutrino absorption cross section. Another ingredient is the partial polarization of the system, which is represented by the spin asymmetry A.

In Fig. 6, we present our result for the absorption neutrino mean free path as a function of the density, at a temperature $T = 15$ MeV, for two values of the magnetic field, $B = 10^{17}$ G and $B = 10^{18}$ G and for three different angles of the incoming neutrino. If we compare these results with the dispersions ones (see Fig. 10 in [38]), we notice that the mean free path shows the same qualitative behavior. But, at variance with the dispersion case, the magnitude of the absorption mean free path has a strong dependence on the magnetic field. From $B = 10^{17}$ G to $B = 10^{18}$ G there is an important reduction in the mean free path. The reason for this reduction is magnetic dependence of the phase space for final states. An increase of this phase space results in an increase of the cross section and consequently a reduction in the mean free path. As we

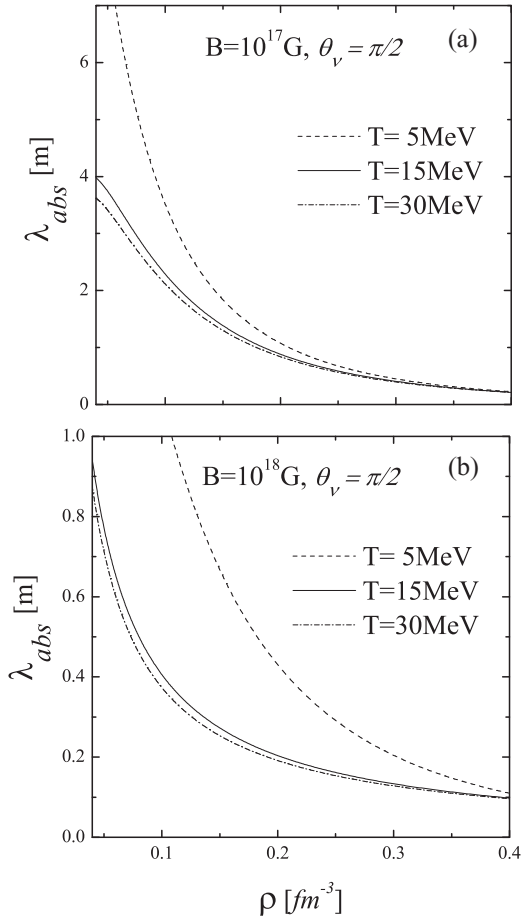

FIG. 7. The absorbtion neutrino mean free path for three different values for the temperature. As in Fig. 6, panels (a) and (b) show the results for magnetic field intensities $B = 10^{17}$ G and $B = 10^{18}$ G, respectively, using the same approximation for the momentum of the incoming neutrino.

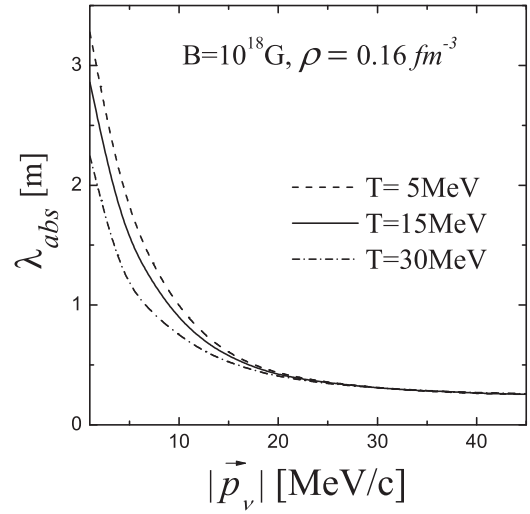

FIG. 8. The absorbtion neutrino mean free path as a function of the momentum of the incoming neutrino $|\vec{p}_\nu|$, for $\theta_\nu = \pi/2$. We have chosen three values for the temperature.

have already discussed, when the magnetic field grows, the number of Landau levels which contribute to the cross section decreases. But the degeneracy of the levels, given by $eBA/2\pi$, grows. Therefore, for increasing values of the magnetic field there is some kind of competition between the increase of the final phase space due to the degeneracy and the reduction in the number of Landau levels. From our numerical results, it turns out that within a range for the magnetic field from $B = 10^{16}$ G up to $B = 10^{18}$ G, the absorption neutrino mean free path decreases for increasing values of the magnetic field. Referring now to the maximum values for N_p and N_e, we can give only indicative values (see the discussion in Appendix B). For $\rho = 0.16$ fm^{-3}, we have $N_p \simeq 150$ and $N_e \simeq 10$ for $B = 10^{17}$ G, while the values for $B = 10^{18}$ G are $N_p \simeq 15$ and $N_e = 0$.

In the next step, we analyze the temperature dependence of the absorption neutrino mean free path. In Fig. 7, we consider three temperatures: $T = 5$, 15, and 30 MeV, for B $= 10^{17}$ G and B $= 10^{18}$ G. For simplicity, we have plotted only the results for $\theta_\nu = \pi/2$, and for the energy of the neutrino we have used the prescription $|\vec{p}_\nu| = 3T$. Our results show that the temperature dependence is rather weak, especially when compared with the dispersion case. To understand this behavior it is useful to compare the dispersion structure function from Fig. 4(a) in [38] with the absorption ones in Fig. 4 in this work: the area of the absorption structure function decreases instead of increasing. This means that the absorption mean free path should increase for higher temperature values. However, our structure function spreads over a wider energy region as the temperature grows, populating more Landau levels. The increase in the number of Landau levels turns down the value of the mean free path. The combined result is a small decrease in the absorption mean free path with temperature.

The temperature dependence is further explored in Fig. 8, where the neutrino absorption mean free path is depicted as a function of the momentum of the neutrino for three values of the temperature, $B = 10^{18}$ G, density $\rho = 0.16$ fm^{-3}, and $\theta_\nu = \pi/2$. The $|\vec{p}_\nu|$ dependence of the neutrino mean free path shows a qualitative agreement for both the dispersion and absorption reactions. This is because the structure function is larger for larger values of the momentum of the neutrino. For the absorption reaction, for an increasing value for $|\vec{p}_\nu|$ we have more energy in the initial state and therefore more Landau levels contribute to the mean free path. The reduction in the structure function for higher temperatures obviously remains. The interplay among these elements for the absorption reaction results in a neutrino mean free path almost independent of the temperature. This is a particular result and we cannot give a deeper explanation. Having in mind the rule $|\vec{p}_\nu| = 3T$ and going back to Fig. 7, we notice the same result: the mean free path for $T = 5$ MeV ($|\vec{p}_\nu| = 15$ MeV) is clearly separated from the ones for $T = 15$ ($|\vec{p}_\nu| = 45$ MeV) and 30 MeV ($|\vec{p}_\nu| = 90$ MeV), for all densities.

At this point, it is clear that the phase space for the final state in the absorption reaction is very different from the one in the dispersion reaction due to the magnetic field. The magnetic field can be reduced continuously to $B = 0$. In the absence of magnetic field, the phase spaces for absorption

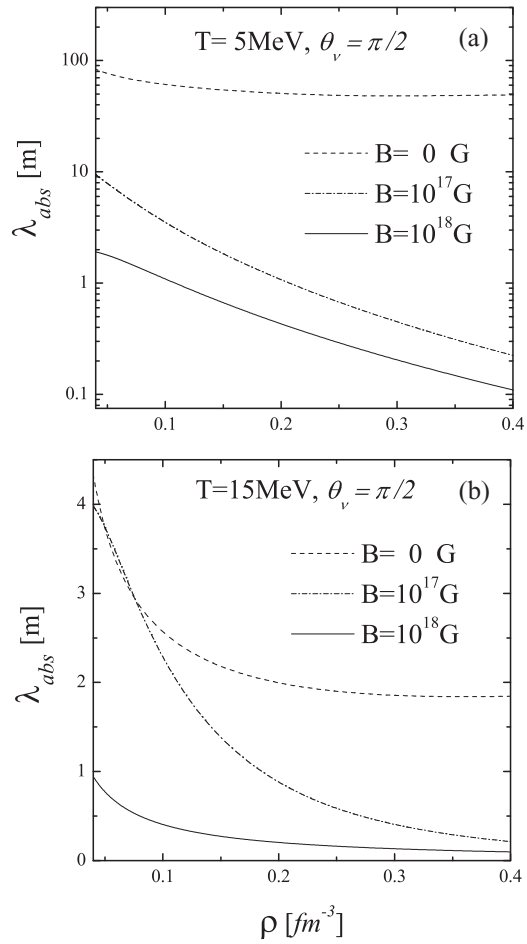

FIG. 9. The absorbtion neutrino mean free path as a function of the density and for three different values for the magnetic field intensity. For the neutrino incoming angle we have employed $\theta_\nu = \pi/2$ and we have used $|\vec{p}_\nu| = 3T$. In panel (a) the temperature is $T = 5$ MeV, while in panel (b) we have $T = 15$ MeV.

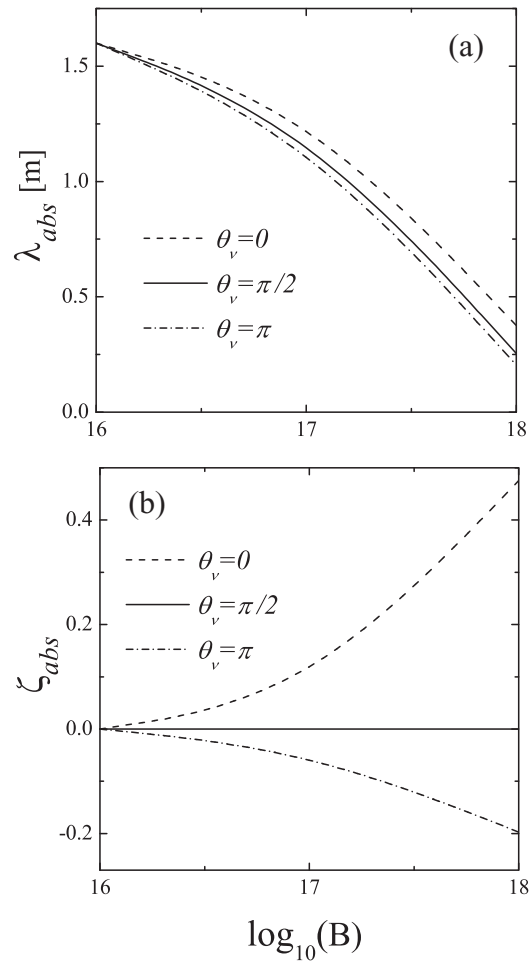

FIG. 10. Dependence on the magnetic field intensity. We have fixed the density at $\rho = 0.16$ fm^{-3} and $T = 15$ MeV. The absorption mean free path is depicted in panel (a) for three angles θ_ν of the incoming neutrino, while in panel (b) we show $\zeta_{\rm abs}$ as defined in Eq. (33), for the same set of angles. The magnetic field intensity B is given in gauss units.

and for the dispersion reaction are the same [17]. In Fig. 9, we show the absorption neutrino mean free path for magnetic fields $B = 0$, 10^{17}, and 10^{18} G, $\theta_\nu = \pi/2$ and two temperatures: $T = 5$ MeV in panel (a) and $T = 15$ MeV in panel (b). Note that in panel (a) we have employed a logarithmic scale for $\lambda_{\rm abs}$. The absorption mean free path for $B = 0$ has a different functional dependence with the density and a very pronounced temperature dependence, consistent with the one for the dispersion reaction. Let us recall that the phase space for the dispersion reaction is barely affected by the magnetic field. It is not a trivial subject to perform the limit from a strong magnetic field to $B = 0$. This discussion goes beyond the scope of the present contribution and we refer the reader to [34,42] for details on how to perform this limit process.

In what follows, we focus on the asymmetry of the neutrino mean free path. In panel (a) in Fig. 10, we show $\lambda_{\rm abs}$ as a function of the magnetic field intensity. This is done at a density $\rho = 0.16$ fm^{-3}, $T = 15$ MeV, and for three angles: $\theta_\nu = 0$, $\pi/2$, and π. As the magnitude of $\lambda_{\rm abs}$ decreases for increasing values of the magnetic field, this figure is somehow misleading because the asymmetry is not clearly seen. Due to this, we have defined the quantity

$$\zeta_{\rm abs} = \frac{\lambda_{\rm abs}(\theta_\nu) - \lambda_{\rm abs}(\theta_\nu = \pi/2)}{\lambda_{\rm abs}(\theta_\nu = \pi/2)}, \tag{33}$$

which gives a more accurate idea of the increase of the asymmetry in the neutrino mean free path. The $\zeta_{\rm abs}$ function is depicted in panel (b) in the same figure. As already discussed, the magnetic field establishes a preference axis in space. Our results show that it is more likely for a neutrino moving antiparallel to the magnetic field ($\theta_\nu = \pi$) to be absorbed, than one which moves parallel to it. Assuming an isotropic production of neutrinos, this implies that more neutrinos are emitted parallel to the magnetic field. In an actual neutron star model, the whole magnetic field cannot be considered as a constant vector field. Our model should be applied locally, according to the geometry of the field.

The asymmetry in the mean free path for both the absorption and dispersion reactions results from the interplay among several elements. Considering the different interactions which

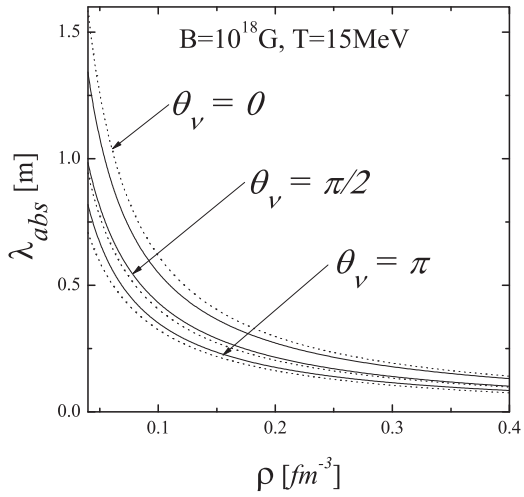

FIG. 11. The absorbtion neutrino mean free path as a function of the density and for three different values for the neutrino incoming angle θ_ν, $B = 10^{18}$ G, and $T = 15$ MeV, where the momentum of the incoming neutrino is taken as $|\vec{p}_\nu| = 3T$. The continuous lines are the case where the spin asymmetry A is arbitrarily taken as zero, while for the dotted lines we employed the not-null A value from our EoS.

take place in the process, we have (i) the results from Table I, giving us information on the weak interaction contribution to the asymmetry in the mean free path; (ii) the strong interaction, which favors the situation $A = 0$; and (iii) the coupling of the magnetic field with protons, neutrons, and electrons, which tends to polarize the system. The balance among these last two elements leads to the equilibrium values for the spin asymmetry A, the effective masses, and the chemical potential. For simplicity, sometimes all these contributions are summarized in one single quantity: the spin asymmetry A. In Fig. 11, we show the mean free path, under the same conditions of panel (b) in Fig. 6, but evaluating the neutrino mean free path putting arbitrarily $A = 0$ (continuous lines in the figure). For comparison we give also the results from Fig. 6 (dotted lines). We can see that the isolated contribution from A does not explain the main contribution to the mean free path asymmetry. Our point here is that the evaluation of the asymmetry in the neutrino mean free path requires a consistent model, starting from the EoS and considering all the just mentioned elements.

As a final point, we include the dispersion contribution to the mean free path. The addition of this contribution gives the total neutrino mean free path, $\lambda_{\rm tot}$:

$$\lambda_{\rm tot} = \left(\frac{1}{\lambda_{\rm abs}} + \frac{1}{\lambda_{\rm dis}}\right)^{-1}. \tag{34}$$

Results for $\lambda_{\rm dis}$ have been taken from [38]. We give our results for this quantity in Figs. 12 and 13. In the first figure we show $\lambda_{\rm tot}$ as a function of the density, for $B = 10^{17}$ and 10^{18} G, three angles for the incoming neutrino, $\theta_\nu = 0$, $\pi/2$, and π, and a temperature $T = 15$ MeV. The second figure has the same variables except for the temperature, where we have employed $T = 30$ MeV. In both figures we have included

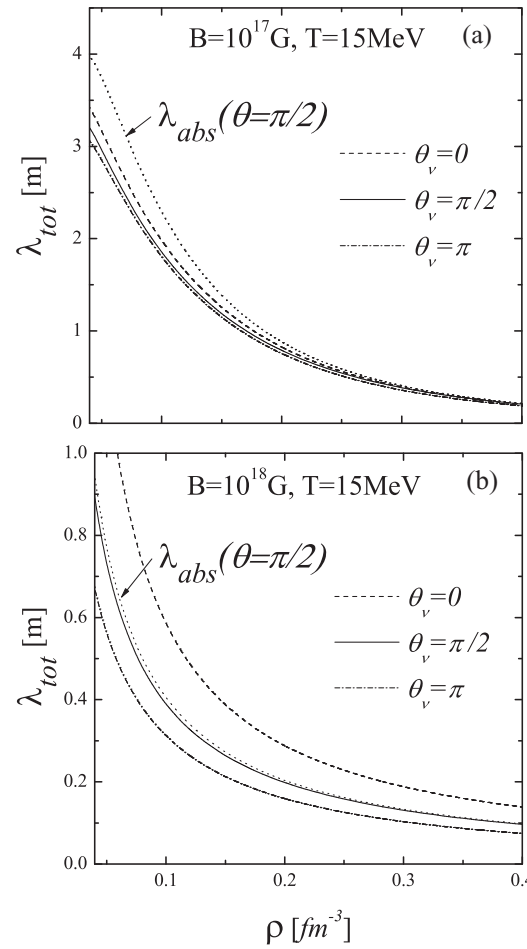

FIG. 12. The total neutrino mean free path for three different values for the neutrino incoming angle θ_ν and for $T = 15$ MeV. As in Fig. 6, panels (a) and (b) show the results for magnetic field intensities $B = 10^{17}$ G and $B = 10^{18}$ G, respectively, using the same approximation for the momentum of the incoming neutrino. For convenience, we show also the absorption neutrino mean free path for $\theta_\nu = \pi/2$.

also $\lambda_{\rm abs}$ for $\theta_\nu = \pi/2$. This is done as a reference of the relative importance of the absorption contribution. Before we go on with our analysis, note that $\lambda_{\rm abs}$ and $\lambda_{\rm dis}$ have very different behaviors for the temperatures and the magnetic fields considered in the present contribution. While $\lambda_{\rm dis}$ has a strong dependence on temperature and its value for $\theta_\nu = \pi/2$ is almost independent of the magnetic field, $\lambda_{\rm abs}$ has a weak dependence on temperature and it decreases for increasing values of the magnetic field. This contrasts with the result for $B = 0$: in this case both $\lambda_{\rm abs}$ and $\lambda_{\rm dis}$ have the same (strong) dependence with temperature and, due to the values of the coupling constants, one has $\lambda_{\rm abs} < \lambda_{\rm dis}$.

By comparing now the panels (a) and (b) in Fig. 12, we notice that the dispersion reaction is as important as the absorption one for $B = 10^{17}$ G, while it is negligible for $B = 10^{18}$ G. This comes as a result of the dependence of $\lambda_{\rm abs}$ on the magnetic field. By doing the same comparison in Fig. 13, we notice that the dispersion contribution becomes more important, due to its strong temperature dependence.

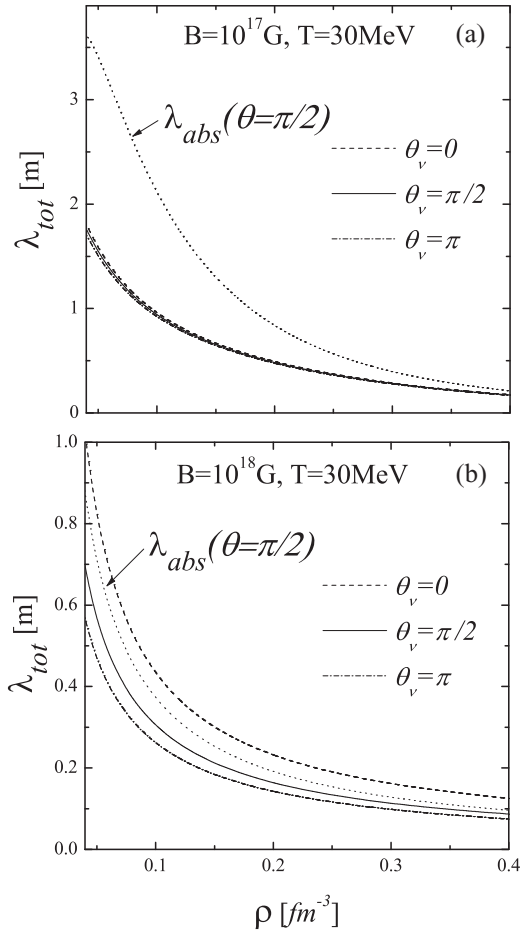

FIG. 13. The same as in Fig. 12, but for $T = 30$ MeV.

We want to finish the discussion of our results by performing a quantitative analysis of the asymmetry. To this end, we define the mean free path asymmetry as

$$\chi_{\rm tot} = \frac{\lambda_{\rm tot}(\theta_\nu = 0) - \lambda_{\rm tot}(\theta_\nu = \pi)}{\langle \lambda_{\rm tot}(\theta_\nu) \rangle}, \tag{35}$$

where we have employed $\langle \lambda_{\rm tot}(\theta_\nu) \rangle \cong [\lambda_{\rm tot}(\theta_\nu = 0) + \lambda_{\rm tot}(\theta_\nu = \pi)]/2$. Note that for the dispersion reaction one has $\langle \lambda_{\rm tot}(\theta_\nu) \rangle = \lambda_{\rm tot}(\theta_\nu = \pi/2)$. We give numerical values for $\chi_{\rm tot}$ in Table II, for three values of the density and for $B = 10^{17}$ and 10^{18} G, with temperatures of $T = 15$ and 30 MeV. As expected, the mean free path asymmetry is more important for the stronger magnetic fields. The reduction in $\chi_{\rm tot}$ for higher values of the density is because the strong interaction becomes more important. Let us recall that the strong interaction favors a nonpolarized system. Some increase of $\chi_{\rm tot}$ at $\rho = 0.40$ fm^{-3} is particular to many of the Skyrme parametrizations. Beyond this difficulty, we have preferred to employ the same parametrization as in [38], in order to make a fair comparison of both contributions to the total mean free path.

TABLE II. Mean free path asymmetry $\chi_{\rm tot}$, as a function of the density for two values of the magnetic field intensity and two values of the temperature.

ρ (fm^{-3})	$\chi_{\rm tot}(B = 10^{17}$ G)		$\chi_{\rm tot}(B = 10^{18}$ G)	
	$T = 15$ MeV	$T = 30$ MeV	$T = 15$ MeV	$T = 30$ MeV
0.050	0.112	0.068	0.740	0.565
0.160	0.088	0.034	0.579	0.479
0.400	0.094	0.042	0.603	0.506

The increase of the temperature leads to a decrease in the mean free path asymmetry. This result seems intuitively correct, as temperature reduces the spin asymmetry A. However, it is convenient to give some details on the origin of this results. In first place, $\lambda_{\rm abs}$ has a weak temperature dependence. On the other hand, $\lambda_{\rm dis}$ depends strongly on the temperature, but its mean free path asymmetry ($\chi_{\rm dis}$) is rather independent of the temperature. The last element is that the absorption mean free path asymmetry is bigger than the dispersion one. This is because in the absorption reaction we deal with charged particles which have a stronger interaction with the magnetic field. Now, as temperature grows, the $\lambda_{\rm dis}$ contribution to $\chi_{\rm tot}$ becomes more important, which leads to smaller values for $\chi_{\rm tot}$, which explains the temperature dependence of our results in this table.

Regarding the use of other EoS, we refer to our previous work [38], in which we also used the BHF model, as mentioned at the beginning of this section. There is a qualitative agreement between the two models for the dispersion reaction. To implement the BHF model for the absorption reaction, one has to evaluate Eq. (28), using the single-particle energies, the chemical potential, and the spin asymmetry A from the BHF model (which are the same as for the dispersion reaction). Numerically, this is much more involved than for the Skyrme model, as in this case the structure function in Eq. (29) [or more specifically in Eq. (C4)], should be evaluated numerically for each value of the N_p and N_e quantum numbers. As a general consideration, by inspection of Fig. 3 in [38], the magnitude of the spin asymmetry A takes smaller values for the BHF model, which means that the asymmetry in the neutrino mean free path will be also smaller if we employ the BHF model.

In the last point for this section, we make some comparison with other works. We start with the work of Shinkevich and Studenikin [34]. This work makes a similar analysis, but using a relativistic framework in free space. In free space, it is employed the total cross section instead of the mean free path. The spin asymmetry A (named S in that work), is taken as an input of the model (i.e., it is not explicitly evaluated). The spin asymmetry is incorporated in their results by making the replacement $s_n \to A$. In the absence of dense medium, this replacement leads to the correct expression. We have an overall agreement with their results, having in mind that in our case the effect of the dense medium is important and the comparison is only qualitative. In our case, a dense medium imposes restrictions on the available phase space, which depends on the temperature. The net effect is a smoothing of the results in relation to theirs.

In the work by Baiko and Yakovlev [32], a formalism similar to ours is employed. However, they focus on very low temperatures, the scope of their paper being different

from ours. To the best of our knowledge perhaps the most complete analysis on the subject has been made by Maruyama *et al.* [37]. We should quote that we have obtained a general agreement with all these papers. What sets us apart from the other works is the treatment we make of the equation of state. We have determined the EoS with a magnetic field and from this we obtain spin-dependent single-particle energies and a chemical potential which lead to specific values for ρ_+ and ρ_-, the densities of neutrons with spin up and down, respectively. Even though the spin asymmetry A appears explicitly in the expression for the cross section, an accurate evaluation of the structure function requires single particles and chemical potential consistent with the value of the magnetic field.

Finally, as our work employs the formalism for the cross section from the work by Arras and Lai [42], we make some comments about this work. The scope of the work is different than ours. In [42], a formalism of neutrino transport in the presence of magnetic field is developed and explicit expressions are derived for the neutrino flux of the Boltzmann transport equation. Unlike our work in which we attach great importance to the EoS, in [42] no EoS is discussed. The work focuses on developing a set of analytical expressions of astrophysical interest. To obtain their expressions, certain approximations are used, which we will not discuss here. Unfortunately, numerical results for the neutrino mean free path are not discussed, which precludes a comparison.

IV. SUMMARY AND CONCLUSIONS

In this work we have evaluated the neutrino mean free path for the absorption reaction $\nu + n \to e^- + p$, in hot dense neutron matter under a strong magnetic field. First, we evaluated an EoS using the Hartree-Fock model with an LNS Skyrme interaction. As mentioned, we have a proton and an electron as final state. Being charged particles in a magnetic field, their quantum state is partially quantized, showing the so-called Landau levels. Due to this quantization, the phase space of final states is quite different from that of the same reaction but in the absence of a magnetic field. This contrasts with the scattering reaction ($\nu + n \to \nu' + n'$), where the phase spaces of final states are very similar. While for $B = 0$ the absorption reaction is always more important than the dispersion one, when $B \neq 0$, the situation is different: $\lambda_{\rm abs}$ has a weak dependence on the temperature and decreases when the magnetic field grows, while $\lambda_{\rm dis}$ has a strong dependence on the temperature (it decreases for growing values of T), and for $\theta_\nu = \pi/2$ is almost independent of the magnetic field. Therefore, in the presence of a strong magnetic field, either $\lambda_{\rm abs}$ or $\lambda_{\rm dis}$ can be the dominant contribution depending on the temperature. As a corollary of this behavior $\lambda_{\rm abs}$ can be important for low temperatures as long as the magnetic field is strong.

For a not-null magnetic field, the neutrino mean free path depends on the angle between the momentum of the neutrino and the magnetic field (which we take as the $\hat{z}$ axis). Let us recall that we consider the magnetic field to be locally constant. Keeping this in mind, this establishes a preferred direction in space resulting in an asymmetrical emission. This asymmetry is the result of the interplay among the weak, strong, and electromagnetic interactions. The weak interaction is responsible for the reaction $\nu + n \to e^- + p$, giving as a result a transition matrix element which depends on the spin of the particles involved. On the other hand, we need a model for the strong interaction to solve the EoS, together with the electromagnetic coupling of the neutron magnetic moment with the magnetic field. From the EoS we obtain a partially polarized system. This information is contained in the single-particle energies, the chemical potential, and the neutron spin asymmetry A, needed for the evaluation of the neutrino mean free path. As already mentioned, the EoS gives us the equilibrium situation between the strong interaction (which favors $A = 0$) and the coupling to the magnetic field ($A \to -1$). For more complex systems, one needs a spin asymmetry for each particle which couples to the magnetic field. For instance, in [49] an EoS was developed for a system of protons and neutrons (at a fixed fraction of protons) where two asymmetries (one for neutrons and another one for protons) were discussed.

It is worth mentioning that the actual problem of the angular distribution of the emitted neutrinos from a neutron star with a strong magnetic field is a much more complex issue. We believe that the two reactions considered in this work are two of the most relevant reactions to understand this problem. To accomplish the bigger goal of modeling a neutron star, one needs several elements. First, one needs a model for the magnetic field distribution. Due to the scale of the reactions, a locally constant field is a good approximation. But for the emission from the whole star, one should care about a model for the magnetic field distribution. Second, a model for the composition and mass distribution of the star is needed. Perhaps the simplest realistic model for star matter consists of protons, neutrons, and electrons in β equilibrium and charge neutrality. More elaborate models include hyperons and leptons (beyond the electron). In this case, we also have Landau levels in the initial state and the scheme must be extended for these conditions. Unlike what happens for the $B = 0$ case and to the best of our knowledge, there is no EoS available for matter at β equilibrium within a strong magnetic field, where single-particle energies, chemical potentials, and the spin asymmetry for each particle are explicitly discussed. In addition to and beyond the reactions considered in this work, there are other reactions which should be considered (see for instance [16,42]).

Our results shows that the shortest neutrino mean free path is obtained for neutrinos moving antiparallel to the magnetic field. As a consequence it is expected that the flux of emitted neutrinos parallel to the magnetic field is bigger than the one in the opposite direction. In Eq. (35) we have defined the mean free path asymmetry $\chi_{\rm tot}$, in order to account for this asymmetry in a quantitative way. We have obtained rather big values for $\chi_{\rm tot}$. However, it would be speculative to draw a conclusion from these values: as discussed in the above paragraph, a model for the geometry of the magnetic field, the local density and temperature, together with the actual composition of a neutron star should be considered. In any case, we understand that in the search for an explanation for the pulsar kick problem, this asymmetry cannot be ignored.

In this work we have shown a self-consistent treatment of the mean free path for neutrinos, starting from the EoS and putting special emphasis in its asymmetry. Both the weak transition matrix element and the EoS contribute to the asymmetry in the neutrino mean free path. We have employed pure hot dense neutron matter due to it simplicity and because it is a reasonable assumption that this model represents one important contribution to the problem. Nuclear correlations beyond the mean field could have a relevant effect on the mean free path and its asymmetry. One way to deal with these correlations is the so-called ring approximation (see for instance [50,51]). But there are other correlations that can be also important. From this, our next aim is to analyze the role of nuclear correlations beyond the mean field on the neutrino mean free path.

ACKNOWLEDGMENTS

We thank Isaac Vidaña for his careful reading of our manuscript. This work was partially supported by the CONICET, Argentina, under Contract No. PIP00273.

APPENDIX A: WAVE FUNCTIONS AND PHASE SPACE SUMMATION

We give and discuss the wave function for electrons, protons, neutrons, and neutrinos. We employ cylindrical coordinates (ρ, ϕ, z). For convenience we also show the single particle energies and explicit expressions for $\int d\Pi_N$ (the state summation for particle N). All particle wave functions are normalized within a volume $V = L\mathcal{A}$, where L is the length along the z axis and $\mathcal{A}$ is the area in the (ρ, ϕ) plane. This is done for convenience and our final results for the mean free path are independent of V. All particles are within a constant magnetic field in the $\hat{z}$ direction, $\boldsymbol{B} = B\hat{k}$. We discuss for each particle the effect of this field.

1. The electron

First we consider the solution of the Dirac equation for an electron within a constant magnetic field B, in the $\hat{z}$ direction. This wave function is derived in full detail in [45]. Our notation is similar to the one in [42]. We reproduce the results below and briefly discuss them. The electron wave function is

$$\Psi_e(\rho, \phi, z, t) = L^{-1/2} e^{i(p_{e,z}z - E_e t)} \left(\frac{eB}{2\pi}\right)^{1/2} e^{i(N_e - R_e)\phi}\, U_e(\rho, \phi), \tag{A1}$$

where the energy is given by

$$E_e = \left(m_e^2 + 2eBN_e + p_{e,z}^2\right)^{1/2}, \tag{A2}$$

where $N_e = 0, 1, 2, \ldots, N_{e,\max}$ is the Landau level index for the energy (the value for $N_{e,\max}$ is discussed in Appendix B), $p_{e,z}$ is the z component of the momentum, and for the spinor $U_e(\rho, \phi)$ we have

$$U_e(\rho, \phi) = \begin{pmatrix} C_1 I_{N_e-1,R_e}(\xi) e^{-i\phi} \\ iC_2 I_{N_e,R_e}(\xi) \\ C_3 I_{N_e-1,R_e}(\xi) e^{-i\phi} \\ iC_4 I_{N_e,R_e}(\xi) \end{pmatrix}, \tag{A3}$$

with $C_1 = \alpha_+ A_+$, $C_2 = \sigma_e \alpha_- A_+$, $C_3 = \sigma_e \alpha_+ A_-$, and $C_4 = \alpha_- A_-$, where

$$\alpha_\pm = \sqrt{\frac{1}{2}\left(1 \pm \sigma_e \frac{p_{e,z}}{\mid \Lambda \mid}\right)}$$

$$A_\pm = \sqrt{\frac{1}{2}\left(1 \pm \frac{m_e}{E_e}\right)}, \tag{A4}$$

with $\mid \Lambda \mid = (p_{e,z}^2 + 2eBN_e)^{1/2}$, and σ_e is the spin projection which is discussed soon. The function $I_{N_e,R_e}(\xi)$ is given by

$$I_{N_e,R_e}(\xi) = \left(\frac{R_e!}{N_e!}\right)^{1/2} e^{-\xi/2} \xi^{(N_e - R_e)/2} \mathcal{L}_{R_e}^{N_e - R_e}(\xi), \tag{A5}$$

with $\xi = eB\rho^2/2$, and for the definition of the Laguerre polynomials $\mathcal{L}_j^i$ we have adopted the one from [52]. The R_e is called the radial quantum number, with values $R_e = 0, 1, 2, \ldots, R_{e,\max}$. The value for $R_{e,\max}$ is discussed soon in this section.

The plane-wave states in the $\hat{z}$ direction ($e^{ip_{e,z}z}$) are limited by the length L. We apply the periodic boundary condition $e^{ip_{e,z}z} = e^{ip_{e,z}(z+L)}$. More explicitly we require that $e^{ip_{e,z}L} = 1 = \cos(p_{e,z}L) + i\sin(p_{e,z}L)$, therefore the allowed wave numbers are

$$p_{e,z} = \frac{2\pi n_z}{L}, \quad n_z = 0, \pm 1, \pm 2, \ldots. \tag{A6}$$

Note also that we take the continuous limit for $p_{e,z}$, where the discrete summation over n_z is replaced by an integral by means of Eq. (A6):

$$\sum_{n_Z=-\infty}^{\infty} \rightarrow \frac{L}{2\pi} \int_{-\infty}^{\infty} dp_{e,z}. \tag{A7}$$

The electron wave function is characterized by four quantum numbers which correspond to four operators: (i) the Hamiltonian (quantum number N_e), (ii) the operator of the projection of the momentum onto the direction of the magnetic field $\hat{p}_{e,z}$ (quantum number n_z), (iii) the operator of the projection of the total angular momentum onto the direction of the magnetic field $\hat{J}_z$ (quantum number $l = N_e - R_e$), and (iv) the longitudinal polarization $\boldsymbol{\sigma} \cdot \boldsymbol{P}$, where $\boldsymbol{P} = \imath\boldsymbol{\nabla} + e\boldsymbol{A}$, $\boldsymbol{A}$ being the vector potential (quantum number $\sigma_e = \pm 1$).

Instead of working with the azimuthal quantum number l, we employ the R_e quantum number. Note that $l = N_e - R_e$ is a integer; this is because in Eq. (A3) a factor $e^{-i\phi/2}$ has been absorbed by the four-vector. The R_e quantum number admits a geometrical interpretation which we do not discuss. We refer the interested reader to [45] for this discussion. From Eq. (A2), the energy does not depend on the R_e quantum number, meaning that the energy levels are degenerate. The degree of the degeneration is given by the maximum value for this quantum number, $R_{e,\max}$.

The degree of the quantum degeneracy of the wave function in Eq. (A1) is independent of the coordinate system used to represent it. We outline the derivation of $R_{e,\max}$ given by Landau and Lifshitz [53], developed in Cartesian coordinates. At this point it is helpful to recall that the classical trajectory of an electron within a constant magnetic field is given by

a circular helix whose axis is parallel to the $\hat{z}$ direction (see for instance Fig. 1, Complement E_{VI} in [54]). In the quantum problem, the state is degenerate with respect to $p_{e,x}$, the $\hat{x}$ component of the linear momentum. We know the y coordinate of the center of the circle in the xy plane, given by $y_0 = -p_{e,x}/eB$, which should lie within the area $\mathcal{A}$, that is, $0 \leqslant y_0 \leqslant L_y$. Using Eq. (A6) but for the x axis, we have $n_x = L_x p_{e,x}/2\pi$. Finally we have $R_{e,\max} = n_{x,\max} = eBL_xL_y/2\pi$ or $R_{e,\max} = eB\mathcal{A}/2\pi$. Note that without a finite volume V, the degree of degeneration would be infinite.

Now we pay attention to the ground state ($N_e = 0$). As the functions I_{-1,R_e} are not well defined, only the spin projection $\sigma_{e0} = -\,\mathrm{sgn}(p_{e,z})$ is allowed (in this case from Eq. (A4), the coefficient $\alpha_+ = 0$). Hence the ground state has spin opposite to the magnetic field.[1] Finally, we consider the state summation $\int d\Pi_e$. This is the sum over all quantum numbers (discrete and continuous). We have

$$\int d\Pi_e = \sum_{N_e=0}^{N_{e,\max}} \sum_{\sigma_e=\pm 1} c(N_e,\sigma_e) \sum_{R_e=0}^{R_{e,\max}} \frac{L}{2\pi} \int_{-\infty}^{\infty} dp_{e,z}, \quad \text{(A8)}$$

where the function $c(N_e,\sigma_e) = 1 - \delta_{N_e,0}\delta_{\sigma_e,-\sigma_{e0}}$, with $\sigma_{e0} = -\,\mathrm{sgn}(p_{e,z})$. This function is equal to 1, except for its null value when $N_e = 0$ and $\sigma_e = -\sigma_{e0}$. This is needed because of the discussion given in the preceding paragraph. In Appendix B, we discuss the value of $N_{e,\max}$.

2. The proton

For the proton, we employ a nonrelativistic wave function. Being a spin-1/2 charged particle, the proton also has Landau levels. But it would be wrong to take the electron wave function, change the mass and the charge, and take the nonrelativistic limit. For the electron case, one could arrange the spinors so that the energy depends only on N_e. The anomalous magnetic moment of the proton does not allow this procedure. We have performed the nonrelativistic calculation of the proton wave function within a constant magnetic field and we have obtained the same result as in [42]:

$$\Psi_p(\rho,\phi,z,t) = L^{-1/2} e^{i(p_{p,z}z - E_p t)} \left(\frac{eB}{2\pi}\right)^{1/2} e^{i(R_p - N_p)\phi}\, U_p(\rho), \quad \text{(A9)}$$

where

$$U_p(\rho) = \begin{pmatrix} \delta_{s_p,+1} I_{R_p,N_p}(\xi) \\ \delta_{s_p,-1} I_{R_p,N_p}(\xi) \\ 0 \\ 0 \end{pmatrix}. \quad \text{(A10)}$$

The nonrelativistic expression for the energy of the proton is

$$E_p = m_p + \frac{p_{p,z}^2}{2m_p} + \frac{eB}{m_p}\left(N_p + \frac{1}{2}\right) - s_p \mu_{Bp} B, \quad \text{(A11)}$$

where $\mu_{Bp} = 2.793\mu_N$ and $N_p = 0, 1, 2, \ldots, N_{p,\max}$, is the energy level quantum number for the proton Landau state and $N_{p,\max}$ is discussed in Appendix B. The meaning of $I_{R_p,N_p}(\xi)$, ξ, and R_p are the same as for the electron. In particular, $R_p = 0, 1, 2, \ldots, R_{p,\max}$, with $R_{p,\max} = R_{e,\max}$.

For the proton state summation we have

$$\int d\Pi_p = \sum_{N_p=0}^{N_{p,\max}} \sum_{R_p=0}^{R_{p,\max}} \sum_{s_p=\pm 1} \frac{L}{2\pi} \int_{-\infty}^{\infty} dp_{p,z}. \quad \text{(A12)}$$

As for the electron, we discuss in Appendix B the value of $N_{p,\max}$.

3. The neutron

We employ a nonrelativistic wave function for the neutron. Let us recall that we are considering pure hot neutron matter for the reaction $\nu + n \to e^- + p$, within a strong magnetic field. Neutrons are partially polarized and this information is in the neutron wave function. In unpolarized matter, one makes an average over the spin up and down contributions, $|u\rangle$ and $|d\rangle$, respectively. For polarized matter, we employ a single mixed spin wave function $|\chi_n\rangle$ (for details see Appendix B in [38]),

$$|\chi_n\rangle = \sqrt{\frac{1+A}{2}}\,|u\rangle + \sqrt{\frac{1-A}{2}}\,|d\rangle, \quad \text{(A13)}$$

where A is the spin asymmetry as defined in Eq. (5). The mean value of the spin projection operator $\hat{S}_z$ using this wave function is

$$\langle\chi_n|\hat{S}_z|\chi_n\rangle = A\,\frac{\hbar}{2}, \quad \text{(A14)}$$

which is the same as the mean value of the spin projection operator for the whole system, as required by the mean value for a mixed wave function [54]. In what follows, we employ the neutron spin wave function in Eq. (A13) for the evaluation of the cross section:

$$\Psi_n(\rho,\phi,z,t) = (V)^{-1/2} e^{i(\vec{p}_n\cdot\vec{r} - E_n t)}\, U_n, \quad \text{(A15)}$$

where

$$U_n = \sqrt{\frac{1+A}{2}}\,\delta_{s_n,+1}\begin{pmatrix}1\\0\\0\\0\end{pmatrix} + \sqrt{\frac{1-A}{2}}\,\delta_{s_n,-1}\begin{pmatrix}0\\1\\0\\0\end{pmatrix}. \quad \text{(A16)}$$

The inclusion of $\delta_{s_n,+1}$ and $\delta_{s_n,-1}$ is done for convenience. We repeat the expression for the energy from Eq. (6):

$$E_n = m_n + \frac{p_n^2}{2m_{s_n}^*} - s_n\mu_{Bn}B + \frac{v_{s_n}}{8}.$$

Finally, for the neutron, we have

$$\int d\Pi_n = \sum_{s_n=\pm 1} \frac{1}{(2\pi)^3} \int d^3p_n. \quad \text{(A17)}$$

[1] Just for clarity, we simplify this point by giving the nonrelativistic limit. In this case, we have $N_e = n + 1/2 + \tilde{s}_e$, with $n = 0, 1, 2, \ldots$ and $\tilde{s}_e = \pm 1/2$. First we consider the ground state $N_e = 0$, therefore $n = 0$ and $\tilde{s}_e = -1/2$, having only one possible spin projection. If we take a fixed value for N_e, with the condition that it is not equal to zero, then we can have the two spin projections: $N_e = n + 1/2 + |\,\tilde{s}_e\,|$ and $N_e = n' + 1/2 - |\,\tilde{s}_e\,|$, with $n' = n + 1$.

4. The neutrino

We are considering massless neutrinos which are left handed (or polarized). In this case, for a neutrino with momentum $\vec{p}_\nu$, its energy is $\mid \vec{p}_\nu \mid$ and the wave function is given by

$$\Psi_\nu(\rho, \phi, z, t) = V^{-1/2} e^{i(\vec{p}_\nu \cdot \vec{r} - |\vec{p}_\nu| t)} U_\nu(\theta_\nu), \tag{A18}$$

where,

$$U_\nu(\theta_\nu) = \frac{1}{\sqrt{2}} \begin{pmatrix} -\sqrt{1-\cos(\theta_\nu)} \\ \sqrt{1+\cos(\theta_\nu)} \\ \sqrt{1-\cos(\theta_\nu)} \\ -\sqrt{1+\cos(\theta_\nu)} \end{pmatrix}, \tag{A19}$$

where θ_ν is the polar angle for $\vec{p}_\nu$ and we take $\phi_\nu = 0$ for the azimuthal angle. As we are considering a single neutrino with its wave function given by Eq. (A18), no summation over the neutrino state is needed.

APPENDIX B: ESTIMATION FOR $N_{p,\max}$ AND $N_{e,\max}$

In this Appendix we explain why the summation over the quantum numbers N_p and N_e runs up to finite maximum values. This is a consequence of the conservation of the energy. Let us call $E_i = E_\nu + E_n$ and $E_f = E_e + E_p$ the initial and final energies, respectively. The energy conservation ($E_i = E_f$) is expressed by the corresponding δ function in Eq. (C1). All single-particle energies are positive, and for the benefit of the reader we rewrite them here for dense pure neutron matter:

$$\begin{aligned} E_n &= m_n + \frac{p_n^2}{2m_{s_n}^*} - s_n \mu_{Bn} B + \frac{v_{s_n}}{8}, \\ E_\nu &= |p_\nu|, \\ E_p &= m_p + \frac{p_{p,z}^2}{2m_p} + \frac{eB}{m_p}\left(N_p + \frac{1}{2}\right) - s_p \mu_{Bp} B, \\ E_e &= \left(m_e^2 + 2eBN_e + p_{e,z}^2\right)^{1/2}. \end{aligned}$$

The key point which determines finite values for $N_{p,\max}$ and $N_{e,\max}$ is that the neutron is in a dense medium. The equilibrium conditions of particles in a dense medium limit their maximum energy. This information is contained in the function $f_{s_n}(E_n, \mu_n, T)$ [see Eq. (C1)]. To make our point clearer, let us consider the $T \to 0$ limit, and we neglect the interaction among neutrons ($m_{s_n}^* \to m_n$ and $v_{s_n} \to 0$). In that case, we have

$$\lim_{T\to 0} f_{s_n}(E_n, \mu_n, T) = \theta(\mu_n - E_n). \tag{B1}$$

The Fermi energy is defined by the relation, $E_F(p_F) = \mu_n$, where p_F is the Fermi momentum. The value for μ_n is obtained from the EoS. The maximum value for the initial energy is then

$$E_{i,\max} = |p_\nu| + m_n + \frac{p_F^2}{2m_n} + \mid \mu_{Bn} B \mid . \tag{B2}$$

The values for $|p_\nu|$ and B are inputs of our calculation. This means that $E_{i,\max}$ cannot take arbitrarily big values. The situation for a free neutron is different, since its kinetic energy can take any value. We turn now to E_f:

$$\begin{aligned} E_f =& m_p + \frac{p_{p,z}^2}{2m_p} + \frac{eB}{m_p}\left(N_p + \frac{1}{2}\right) \\ & - s_p \mu_{Bp} B + \left(m_e^2 + 2eBN_e + p_{e,z}^2\right)^{1/2}. \end{aligned} \tag{B3}$$

There is no Fermi sea for protons nor one for electrons within our model of pure neutron matter. This means that both $\mid p_{p,z} \mid$ and $\mid p_{e,z} \mid$ can take values within the range $[0, \infty)$, but the constraint $E_i = E_f$ limits this range. We focus on $N_{p,\max}$ and $N_{e,\max}$. For fixed values for B, $p_{p,z}$ and $p_{e,z}$, E_f grows for increasing values for N_p and N_e. To evaluate $N_{p,\max}$ we put $p_{p,z} = p_{e,z} = 0$ and $N_e = 0$. By solving the equation $E_{i,\max} = E_f(p_{p,z} = 0, p_{e,z} = 0, N_e = 0)$, we have

$$\begin{aligned} N_{p,\max} = \frac{m_p}{eB}\Bigg(& \frac{p_F^2}{2m_n} + m_n - m_p - m_e \\ & + |p_\nu| + \mid \mu_{Bn} B \mid + \mid \mu_{Bp} B \mid - \frac{eB}{2m_p}\Bigg). \end{aligned} \tag{B4}$$

The same analysis can be done for $N_{e,\max}$, where now we use $N_{p,\max} = 0$. From the right-hand side of this expression one takes the integer part.

Only when $T = 0$ can we show an analytical expression for $N_{p,\max}$ (or $N_{e,\max}$). This is because $f_{s_n}(E_n, \mu_n, T)$ as a function of p_n decreases exponentially when $E_n(p_n) > \mu_n$, but there is no defined value of p_n for which the function is zero. Note that the temperature changes continuously, meaning that for all practical purposes the result from Eq. (B4) remains valid for $T \approx 0$, although we no longer have the step function from Eq. (B1). This does not mean that we cannot give values for $N_{p,\max}$ and $N_{e,\max}$. This is easily implemented numerically: we sum up $N_{p,\max}$ and $N_{e,\max}$ up to values where the mean free path does not change. In addition, from Eq. (C2) we notice that E_n depends also on $m_{s_n}^*$ and v_{s_n}, which are functions of the density and the temperature. In the text we give indicative values for $N_{p,\max}$ and $N_{e,\max}$, in the sense that for higher values of these quantum numbers the mean free path does not change.

Alternatively, one can employ a numerical criterion to obtain $N_{p,\max}$ and $N_{e,\max}$ at $T \neq 0$. For instance, we write

$$\frac{f_{s_n}(E_n(p_n = 0), \mu_n, T)}{f_{s_n}(E_n(p_{n,\max}), \mu_n, T)} = 10^{-10}. \tag{B5}$$

By solving this equation for $p_{n,\max}$, one uses this value instead of p_F in Eq. (B4) and obtains $N_{p,\max}$. It is very simple to implement the modifications to include $m_{s_n}^*$ and v_{s_n} and develop an analogous equation for $N_{e,\max}$. The factor 10^{-10} is arbitrary and one should change this factor until the mean free path remains unaltered. In practice, for $T = 5$ MeV the results (for $N_{p,\max}$ and $N_{e,\max}$) are close to those for $T = 0$, while for $T = 30$ MeV the increase is given by a few units of these quantum numbers.

As a final point for this Appendix, we make a brief discussion about the interplay between $N_{p,\max}$ and $N_{e,\max}$. One can take these extreme values and ignore this interplay, as long as one does not care about the efficiency of the numerical code which evaluates the mean free path. To discuss this interplay, we show a simple model. From E_p we retain only

the N_p contribution, $\Delta E_{Np} \equiv N_p eB/m_p$. And we do the same for the electron, $\Delta E_{Ne} \equiv (m_e^2 + 2eBN_e)^{1/2} - m_e$. We define $\Delta E_f \equiv \Delta E_{Np} + \Delta E_{Ne}$ and, just to give an example, we set the maximum possible value for this energy at $\Delta E_f^{\max} = 64$ MeV. We consider two cases: (i) For $B = 10^{18}$ G, we have $\Delta E_{Np=10} = 63$ MeV, but $\Delta E_{Ne=1} = 108$ MeV, which means that no electron Landau level contributes to the cross section and we have to sum N_p from zero up to ten. (ii) For $B = 10^{17}$ G, $\Delta E_{Np=100} = 63$ MeV, and in this case $\Delta E_{Ne=3} = 59$ MeV. Then, we have combinations among the proton and the electron Landau levels: $N_p = 0, 1, 2, \ldots, 100$ and $N_e = 0$; $N_p = 0$ and $N_e = 0, 1, 2, 3$; $N_p = 0, 1$ and $N_e = 0, 1$; etc. Due to the small electron mass, the energy gap is always bigger for the electron.

APPENDIX C: EVALUATION OF THE STRUCTURE FUNCTION S_{s_p,s_n,N_p,N_e}

In this Appendix we evaluate the structure function for the absorption process S_{s_p,s_n,N_p,N_e}. We present a general expression, but at the end of this Appendix we show a simpler expression which is more appropriate for our work. We recall the structure function defined in Eq. (29),

$$\begin{aligned} S_{s_p,s_n,N_p,N_e} = & \int_{-\infty}^{\infty} \frac{dp_{n,z}}{2\pi} \int_{-\infty}^{\infty} \frac{dp_{p,z}}{2\pi} (2\pi)^2 \\ & \times \delta(E_e + E_p - |p_\nu| - E_n) \\ & \times \delta(p_{e,z} + p_{p,z} - p_{\nu,z} - p_{n,z}) \\ & \times f_{s_n}(E_n, \mu_n, T)\left[1 - f_{s_p}(E_p, \mu_p, T)\right], \end{aligned} \tag{C1}$$

where $f_{s_i}(E_i, \mu_i, T)$ has been given in Eq. (4). The single-particle energies E_i and the chemical potentials μ_i should be obtained from a particular model for the medium, which in our case is the Skyrme model (see [40,41] and references therein). Within the Skyrme model, the nucleons single-particle energies for particles in a magnetic field, can be written as,

$$\begin{aligned} E_p &= m_p + \frac{p_{p,z}^2}{2m_{s_p}^*} + \frac{eB}{m_p}\left(N_p + \frac{1}{2}\right) - s_p \mu_{Bp} B + \frac{v_{s_p}}{8} \\ E_n &= m_n + \frac{p_n^2}{2m_{s_n}^*} - s_n \mu_{Bn} B + \frac{v_{s_n}}{8}, \end{aligned} \tag{C2}$$

where μ_{Bp} and μ_{Bn} are the proton and neutron magnetic moments, respectively and N_p indicates the Landau level. The effective masses ($m_{s_p}^*$ and $m_{s_n}^*$), together with the residual terms v_{s_p} and v_{s_n}, depend on the density of the system, and explicit expressions are found in [40,41]. The structure function gives us information on the accessible phase space of protons and neutrons. Even thought we work with neutron matter, the single-particle energies in Eq. (C2) are the ones for proton-neutron matter. We have employed these energies to give a more general expression for the structure function.

We take both the neutrino and the electron energies as in free space (with a magnetic field). We are considering massless neutrinos which are left handed (or polarized). The energy of the electron is taken as

$$E_e = \left(m_e^2 + 2eBN_e + p_{e,z}^2\right)^{1/2}. \tag{C3}$$

Note that due to the particular value for the magnetic moment of the electron, one can arrange the expression so that the energy depends only on N_e.

We now use the delta function representing the momentum conservation in Eq. (C1) to obtain

$$\begin{aligned} S_{s_p,s_n,N_p,N_e} = & \int_{-\infty}^{\infty} dp_{n,z}\, \delta(E_e + E_p - |p_\nu| - E_n) f_{s_n}(E_n, \mu_n, T) \\ & \times \left[1 - f_{s_p}(E_p, \mu_p, T)\right], \end{aligned} \tag{C4}$$

where $p_{p,z} = p_{\nu,z} + p_{n,z} - p_{e,z}$. By assigning impulse values to the lines in the diagram in Fig. 1, energy-momentum conservation allow us to write

$$\begin{aligned} q_0 &= |p_\nu| - E_e, \\ q_z &= p_{\nu,z} - p_{e,z}, \\ p_{p,z} &= p_{n,z} + q_z. \end{aligned} \tag{C5}$$

Using these expressions we replace the energy and the z-momentum component of the electron by q_0 and q_z. The remainder integral in Eq. (C4) can be done by solving the energy-conservation equation

$$E_e + E_p - |p_\nu| - E_n = 0, \tag{C6}$$

which in fact is a polynomial of second order in $p_{n,z}$. After some algebra, we have

$$\alpha_n p_{n,z}^2 + \beta_n p_{n,z} + \gamma_n = 0, \tag{C7}$$

where

$$\begin{aligned} \alpha_n &= \frac{1}{2}\left(\frac{1}{m_{s_p}^*} - \frac{1}{m_{s_n}^*}\right), \\ \beta_n &= \frac{q_z}{m_{s_p}^*}, \\ \gamma_n &= -\frac{p_{n,\perp}^2}{2m_{s_n}^*} + \frac{q_z^2}{2m_{s_p}^*} - m_n + m_p - q_0 \\ &\quad + \frac{eB}{m_p}\left(N_p + \frac{1}{2}\right) - s_p \mu_{Bp} B \\ &\quad + s_n \mu_{Bn} B + \frac{1}{8}\left(v_{s_p} - v_{s_n}\right), \end{aligned} \tag{C8}$$

We recall that $p_{n,\perp} = \sqrt{p_{n,x}^2 + p_{n,y}^2}$. The energy-momentum of the neutrino and the electron enter into the structure function through the external quantities q_0 and q_z. This means that our expression for the structure function remains valid also for a dense system built up from protons, neutrons, electrons, and neutrinos. Energy conservation can now be rewritten as

$$\begin{aligned} \delta(E_p - E_n - q_0) = & \frac{1}{\left(\beta_n^2 - 4\alpha_n^2\gamma_n^2\right)^{1/2}} \\ & \times [\delta(p_{n,z} - p_{n,z}^+) + \delta(p_{n,z} - p_{n,z}^-)], \end{aligned} \tag{C9}$$

where $p^{\pm}_{n,z}$ are the roots of Eq. (C7). Finally, the expression for the structure function is given by

$$S_{s_p,s_n,N_p,N_e} = \frac{1}{\left(\beta_n^2 - 4\alpha_n^2\gamma_n^2\right)^{1/2}}\Big[f_{s_n}(E_n,\mu_n,T) \times \left[1 - f_{s_p}(E_p,\mu_p,T)\right]|_{p_{n,z}=p^+_{n,z}} + f_{s_n}(E_n,\mu_n,T)\left[1 - f_{s_p}(E_p,\mu_p,T)\right]|_{p_{n,z}=p^-_{n,z}}\Big]. \tag{C10}$$

In particular, in this work we consider pure neutron matter. Therefore, in Eqs. (C2), (C8), and (C10), we have to replace $f_{s_p}(E_p,\mu_p,T) \to 1$, $m^*_{s_p} \to m_p$, and $v_{s_p} \to 0$, obtaining

$$S_{s_p,s_n,N_p,N_e} = \frac{1}{\left(\beta_n^2 - 4\alpha_n^2\gamma_n^2\right)^{1/2}}\Big[f_{s_n}(E_n,\mu_n,T)|_{p_{n,z}=p^+_{n,z}} + f_{s_n}(E_n,\mu_n,T)|_{p_{n,z}=p^-_{n,z}}\Big]. \tag{C11}$$

As mentioned in the text, we should recall that the structure function is a function of many variables. For simplicity, we show explicitly only the discrete variables, but it also depends on q_0, q_z, $p^2_{n,\perp}$, $m^*_{s_p}$, $m^*_{s_n}$, μ_p, μ_p, T, and B.

Another limit is when $m^*_{s_p} = m^*_{s_n} = m_N$. In this case, we have $\alpha_n = 0$, and Eq. (C7) reduces to

$$\beta_n\, p_{n,z} + \gamma_n = 0, \tag{C12}$$

that is, $p_{n,z} = -\gamma_n/\beta_n$ and

$$\frac{1}{\left(\beta_n^2 - 4\alpha_n^2\gamma_n^2\right)^{1/2}} \to \frac{m_N}{|\,q_z\,|}, \tag{C13}$$

and the structure function is

$$S_{s_p,s_n,N_p,N_e} = \frac{m_N}{|\,q_z\,|}\, f_{s_n}(E_n,\mu_n,T) \times \left[1 - f_{s_p}(E_p,\mu_p,T)\right]|_{p_{n,z}=-\gamma_n/\beta_n}, \tag{C14}$$

which is the same expression as in Eq. (E2) in [42].

As a final comment on this Appendix, we should mention that for $\beta_n^2 - 4\alpha_n^2\gamma_n^2 = 0$ [or equivalently for $q_z = 0$ in Eq. (C14)], there is a point for which the structure function is undefined. This is because at this point the energy has a double pole ($p^+_{n,z} = p^-_{n,z}$).

[1] H. A. Bethe, Rev. Mod. Phys. **62**, 801 (1990).
[2] H.-Th. Janka and E. Müller, Astron. Astrophys. **306**, 167 (1996).
[3] A. Burrows, Nature (London) **403**, 727 (2000).
[4] A. Burrows and J. M. Lattimer, Astrophys. J. Suppl. **307**, 178 (1986).
[5] H.-Th. Janka and E. Müller, Astrophys. J. Lett. **448**, L109 (1995).
[6] D. G. Yakovlev, A. D. Kaminker, O. Y. Gnedin, and P. Haensel, Phys. Rep. **354**, 1 (2001).
[7] Y. A. Shibanov and D. G. Yakovlev, Astron. Astrophys. **309**, 171 (1996).
[8] D. G. Yakovlev and C. J. Pethick, Annu. Rev. Astron. Astrophys. **42**, 169 (2004).
[9] D. Tubbs and D. Schramm, Astrophys. J. **201**, 467 (1975).
[10] R. F. Sawyer, Phys. Rev. D **11**, 2740 (1975).
[11] N. Iwamoto and C. J. Pethick, Phys. Rev. D **25**, 313 (1982).
[12] S. O. Bäckman, C. G. Källman, and O. Sjöberg, Phys. Lett. B **43**, 263 (1973).
[13] P. Haensel and A. J. Jerzak, Astron. Astrophys. **179**, 127 (1987).
[14] C. J. Horowitz and K. Wehrberger, Nucl. Phys. A **531**, 665 (1991).
[15] S. Reddy and M. Prakash, Astrophys. J. **478**, 689 (1997).
[16] S. Reddy, M. Prakash, and J. M. Lattimer, Phys. Rev. D **58**, 013009 (1998).
[17] S. Reddy, Ph.D. thesis, State University of New York at Stony Brook, 1998.
[18] S. Reddy, M. Prakash, J. M. Lattimer, and J. A. Pons, Phys. Rev. C **59**, 2888 (1999).
[19] A. Burrows and R. F. Sawyer, Phys. Rev. C **58**, 554 (1998).
[20] J. Navarro, E. S. Hernández, and D. Vautherin, Phys. Rev. C **60**, 045801 (1999).
[21] C. Shen, U. Lombardo, N. Van Giai, and W. Zuo, Phys. Rev. C **68**, 055802 (2003).
[22] J. Margueron, I. Vidaña, and I. Bombaci, Phys. Rev. C **68**, 055806 (2003).
[23] A. Reisenegger, in Proceedings of the International Workshop on Strong Magnetic Fields and Neutron Stars, La Habana, Cuba, April 7–12, 2003 (unpublished), arXiv:astro-ph/0307133.
[24] R. C. Duncan and C. Thompson, Astrophys. J. **392**, L9 (1992).
[25] I. Lerche and D. N. Schramm, Astrophys. J. **216**, 881 (1977).
[26] A. Kusenko and G. Segrè, Phys. Rev. Lett. **77**, 4872 (1996).
[27] Dong Lai and Yong-Zhong Qian, Astrophys. J. **495**, L103 (1998); **505**, 844 (1998).
[28] G. S. Bisnovatyi-Kogan, Astron. Astrophys. Trans. **3**, 287 (1993).
[29] B. Cheng, D. N. Schramm, and J. W. Truran, Phys. Lett. B **316**, 521 (1993).
[30] G. S. Bisnovatyi-Kogan, arXiv:astro-ph/9707120.
[31] C. J. Horowitz and G. Li, Phys. Rev. Lett. **80**, 3694 (1998).
[32] D. A. Baiko and D. G. Yakovlev, Astron. Astrophys. **342**, 192 (1999).
[33] D. Chandra, A. Goyal, and K. Goswami, Phys. Rev. D **65**, 053003 (2002).
[34] S. Shinkevich and A. Studenikin, Pramana J. Phys. **65**, 215 (2005).
[35] V. L. Kauts, A. M. Savochkin, and A. I. Studenikin, Phys. At. Nucl. **69**, 1453 (2006).
[36] T. Maruyama, T. Kajino, N. Yasutake, M.-K. Cheoun, and C.-Y. Ryu, Phys. Rev. D **83**, 081303(R) (2011).
[37] T. Maruyama, N. Yasutake, M.-K. Cheoun, J. Hidaka, T. Kajino, G. J. Mathews, and C.-Y. Ryu, Phys. Rev. D **86**, 123003 (2012).
[38] J. Torres Patiño, E. Bauer, and I. Vidaña, Phys. Rev. C **99**, 045808 (2019).
[39] I. Sagert and J. Schaffner-Bielich, Astron. Astrophys. **489**, 281 (2008).
[40] R. Aguirre, Phys. Rev. C **83**, 055804 (2011).
[41] R. Aguirre, E. Bauer, and I. Vidaña, Phys. Rev. C **89**, 035809 (2014).

[42] P. Arras and D. Lai, Phys. Rev. D **60**, 043001 (1999).
[43] W. Greiner and J. Reinhard, *Field Quantization* (Springer-Verlag, Berlin, 1996).
[44] J. D. Bjorken and S. D. Drell, *Relativistic Quantum Mechanics* (McGraw-Hill, New York, 1964).
[45] A. A. Sokolov and I. M. Ternov, *Synchotron Radiation* (Pergamon, Oxford, 1968).
[46] L. G. Cao, U. Lombardo, C. W. Shen, and N. V. Giai, Phys. Rev. C **73**, 014313 (2006).
[47] R. B. Wiringa, V. G. J. Stoks, and R. Schiavilla, Phys. Rev. C **51**, 38 (1995).
[48] B. S. Pudliner, V. R. Pandharipande, J. Carlson, and R. B. Wiringa, Phys. Rev. Lett. **74**, 4396 (1995).
[49] R. Aguirre and E. Bauer, J. Phys. G **42**, 105101 (2015).
[50] M. A. Pérez-García, Phys. Rev. C **80**, 045804 (2009).
[51] M. A. Pérez-García, Eur. Phys. J. A **44**, 77 (2010).
[52] *Handbook of Mathematical Functions*, edited by M. Abramowitz and I. A. Stegun (Dover, New York, 1972).
[53] L. D. Landau and E. M. Lifshitz, *Quantum Mechanics, Non-Relativistic Theory* (Pergamon, Oxford, 1977).
[54] C. Cohen-Tannoudji, B. Diu, and F. Laloë, *Quantum Mechanics* (John Wiley & Sons, New York, 1977).